Synthesis, characterization, and evaluation of thiocarbazide-functionalized maleic-based polymer for thorium (IV) removal from aqueous solutions

Mohammed Hamza, Eric Guibal, Yuezhou Wei, Shunyan Ning

Synthesis, characterization, and evaluation of thiocarbazide-functionalized maleic-based polymer for thorium (IV) removal from aqueous solutions

Mohammed F. Hamza [a], Eric Guibal [b,*], Yuezhou Wei [a,c,*], Shunyan Ning [a]

[a] School of Nuclear Science and Technology, University of South China, Heng Yang 421001, China
[b] Polymers Composites and Hybrids (PCH), IMT Mines Ales, Alès, France
[c] School of Nuclear Science and Engineering, Shanghai Jiao Tong University, Shanghai, China

A B S T R A C T

The copolymerization of maleic anhydride with *N,N'*-methylenebisacrylamide allowed synthesizing a sorbent (MaMb) that can be functionalized by amidoacidification (for grafting thiocarbazide) (synthesis of TcMaMb). The two sorbents are tested in batch systems for the removal of thorium from aqueous solutions. The characterization of the materials shows similar textural properties and the involvement of amine, carboxylic groups (for MaMb), completed with thiocarbonyl groups (for TcMaMb), in the binding of Th(IV). The maximum sorption occurs at pH close to 4 and the functionalization doubles the maximum sorption capacity (up to 1.36 mmol Th g^{-1}). The sorption isotherm for TcMaMb is fitted by the Langmuir equation (in the case of pristine sorbent, the saturation of the sorbent is not achieved in the tested concentration range making the Freundlich equation more appro-priate). The functionalization improves the uptake kinetics (equilibrium time decreased from 120-180 min to 30 min), and kinetic profiles are fitted by the pseudo-first order rate equation. The selectivity of the sorbent for Th (IV) (and to a certain extent U(VI)) is improved by thiocarbazide grafting, especially at pH above 4 (in the case of equimolar multi-component solutions). The functionalization of MaMb also enhances the selectivity of TcMaMB for thorium when applied to metal removal from pre-treated mining leachate (consistently with synthetic so-lutions). Bound metal can be readily desorbed (complete desorption achieved in 30 min) using 0.3 M HCl so-lutions for both MaMb and TcMaMb sorbents. Another advantage brought by the functionalization concerns the stability of the sorbent at recycling: after five cycles of re-use the sorption efficiency decreases by less than 2 %(meaning less than for MaMb, at about 8 %).

Keywords:

The functionalization of the copolymer of maleic anhydride with *N,N'*-methylenebisacrylamide (MaMb) obtained by the reaction of pristine sorbent with thiocarbazide (TcMaMb) increases the density and diversity of reactive groups

The chemical derivative strongly enhances the sorption properties of the material for Th(IV) removal

Faster kinetics are obtained together with doubled sorption capacity at saturation

The selectivity for thorium binding from complex synthetic solutions (especially at pH >4) and real ore leachate (in acidic solution but with lower sorption capacities) is enhanced by the grafting of thiocarbazide

The readily functionalization of MaMb with thiocarbazide opens promising perspective for the recovery of thorium from complex solutions

1. Introduction

With the energy crisis, a new attention is paid again to the development of nuclear energy. Though the nuclear technology mostly considers uranium as fuel source, a renewed interest has recently been expressed for processes based on thorium nuclear fuel. There are several reasons for promoting the development of this alternative technology: (a) larger abundance of thorium in Earth's crust (about three times more than uranium), (b) associated with ^{235}U, thorium shows higher fissile activity (than U), (c) easy capacity of fast-breeding activity, (d) lower risk of nuclear runaway, and (e) lower production of wastes (though more hazardous) [1]. Another advantage remains the poor applicability of thorium in nuclear weapons. The interest for thorium recovery (and separation) is also driven by environmental implications (minimizing impact), and by mining opportunity (thorium being associated with uranium deposits). Apart the nuclear industry, thorium is incorporated in special alloys (in magnesium-based materials for strength enhancement and creep resistance at high temperature) and specific catalytic systems (as ThO_2).

The recovery of thorium from ores can be processed using the same tools as for the hydrometallurgy of uranium. Acidic leaching remains (after grinding and other pre-treatment steps involving gravimetric and magnetic separations) the most usual method for extracting metal ions from ore mineralization [2–6]. These acidic leachates may contain various metal ions; the valorization of target metals involves the combination of different processes for separating base metals from U(VI), Th (IV) and REEs(III), including solvent extraction [4], precipitation (for example REEs with oxalic acid [7], or playing with complex reagents

* Corresponding authors.
E-mail addresses: eric.guibal@mines-ales.fr (E. Guibal), yzwei@usc.edu.cn (Y. Wei).

[8]). For less concentrated effluents, sorption processes may be more appropriate using ion-exchange and chelating resins [9–13] or extractant-impregnated resins [14–16]. Beaugeard et al. [17] reported the rationales for the design of tailored-made acidic polymers; they reviewed the typology of functional groups with the target metals.

Different strategies have been proposed for designing sorbents for thorium and uranium, including the immobilization of specific extractants into porous supports, the grafting of reactive groups on support backbone, and the co-polymerization processes that contribute to the synthesis of functionalized sorbents. The supports may be inorganic such as silica [18–21] or carbon-based supports (carbon nanofiber [22], multi-walled carbon nanotubes, [23], or graphene oxide nanoribbons [24]). Porous polymers are also very useful for synthesizing efficient sorbents: for example, Amberlite XAD-4 was functionalized for Th(IV) sorption [25], Amberlite XAD-16 was impregnated with carminic acid [26], while Aliquat 336 was immobilized in Chromosorb W [15]. Biosorbent-based sorbents have also been designed for the recovery of these hazardous metal ions: fungal mycelium [27], algal/alginate based materials [28].

Many reactive groups have been considered for the removal of U(VI) and Th(IV) sorbents from aqueous solutions, including amidoxime [29–32], phosphonate [10,33–36], sulfonate [37,38], thiocarbonyl [13], or quaternary ammonium [39,40] groups. One of the keys for enhancing the selectivity and the reactivity may consist in developing bifunctional sorbents [41]. This may be processed by direct grafting of dual reactive groups [30,42–46] or through the impregnation with dual extractants [47]. This is precisely the strategy that was selected for designing two new sorbents applying first a simple reaction between maleic anhydride (MA) and *N*,*N*'-methylenebisacrylamide (MBA) to produce MaMb sorbent, which bears carboxylic groups, tertiary amine groups and maleic ring. Thiocarbazide (CH_6N_4S, also called thiocarbohydrazide, which can be produced by direct reaction of CS_2 with NH_2NH_2) may react with MaMb for producing TcMaMb (a sorbent bearing numerous primary and secondary amine groups, and thiocarbonyl moieties, in addition to the groups hold by MaMb). The sorption of thorium(IV) is investigated using both pristine and functionalized sorbent in order to evaluate the impact of the chemical modification on the sorption behavior (effect of pH, uptake kinetics, sorption performance at equilibrium), but also on metal desorption and sorbent recycling. A specific attention is also paid to the evaluation of sorption selectivity (investigated through the sorption in multi-component synthetic solutions and with real processed mining effluent). The target of the study is to answer the question on the interest of the bifunctionnality in terms of sorption capacities, sorbent stability, and selectivity properties. Is "making the synthesis more complex" (through thiocarbazide functionalization) meaningful and competitive?

2. Materials and methods

2.1. Materials

Maleic anhydride ($C_2H_2(CO)_2O$, 99 %), carbon disulfide (CS_2, > 99.0 %), *N*,*N*'-methylene bis-acrylamide ($CH_2[NHCCH = CH_2]_2$, 99 %), hydrazine hydrate ($NH_2NH_2{\cdot}H_2O$, 50–60 %), formaldehyde (CH_2O; 37.0 %), acetone ($(CH_3)_2CO$; ≥99.5 %), 2-butanone ($CH_3C(O)CH_2CH_3$ ≥ 99 %), sodium hydroxide (NaOH, ≥97.0 %), potassium persulfate ($K_2S_2O_8$, ≥99 %), and hydrochloric acid (HCl, 37 % w/w) were purchased from Sigma-Aldrich (Darmstadt, Germany). Hydrated thorium nitrate ($Th(NO_3)_4{\cdot}H_2O$, ≥99 %) was purchased from Otto-Chemie Pvt. ltd. (Popatwadi, Mumbai, India). Uranyl nitrate hexahydrate ($UO_2(NO_3)_2{\cdot}6H_2O$)* was purchased from SPI Supplies (West Chester, PA, USA). Calcium chloride ($CaCl_2$, ≥99.1 %)* was supplied by Shanghai Makclin Biochemical Co., ltd. (Shanghai, China). Iron (III) sulfate ($Fe_2(SO_4)_3$, 97.0 %)*, zinc chloride ($ZnCl_2$, 98.0 %)*, aluminum chloride ($AlCl_3$, 99.1 %)* and magnesium chloride ($MgCl_2$, 95.0 %)* were purchased from Guangdong Guanghua Sci-Tech Co., ltd. (Guangdong, China). Standard silicon solution (1000 ppm)* was purchased from Guobiao Inspection and Certification Co., ltd. (Beijing, China). Note: * *used in the selectivity experiments*.

2.2. Synthesis of sorbents

2.2.1. Synthesis of thiocarbazide

Thiocarbazide was obtained by the reaction of equimolar amounts of two precursors [48]: 5 g of hydrazine hydrate (50–60 %, w/w; 50 mmol) were added dropwise to 3.8 g of carbon disulfide (50 mmol) in a round bottom flask. The addition was achieved in an ice bath for 90 min, and then the mixture was stirred for further 2 h. The produced precipitate was filtered and dried at 40 °C to produce the thiocarbazide moiety (~5.0 g; i.e., 61.2 mmol) (Scheme 1).

2.2.2. Synthesis of MaMb

MaMb sorbent was obtained through the polymerization of maleic anhydride and *N*,*N*'-methylenebisacrylamide (MBA); This reaction involves a mechanism of redox polymerization [49] (Scheme 1). A homogenous solution of 50 mmol maleic anhydride (4.9 g) and 12.5 mmol of MBA (1.9 g) was dispersed in an anhydrous 2-butanone phase, followed by addition of 0.5 g potassium persulfate (as redox initiator). The reaction mixture was performed in a reactor equipped with a condenser and reflux unit for 10 h, at 80–85 °C. The reaction content was poured in a solution of ethanol:methanol (4:1) for 2 h. The solid precipitate (MaMb) was collected by filtration, washed with ethanol and dried (yielding 6.2 g), under vacuum at 50 °C, for 10 h.

2.2.3. Synthesis of Tc-MaMb

The pristine MaMb sorbent (5 g) was functionalized by grafting thiocarbazide (10 g, ≈95 mmol, in absolute ethanol, 150 mL) (Scheme 1). Two mL of concentrated sulfuric acid were added to the suspension and the reaction was performed at 80 °C for 8 h. The functionalized material (TcMaMb) was collected by filtration, washed with acetone and dried at 60 °C for 10 h. The yield reached 13.5 g (meaning ≈90 % conversion).

2.3. Characterization of materials

Scanning electron microscopy (SEM) and semi-quantitative analysis (by energy dispersive spectroscopy, EDX) were performed using a Phenom ProX-SEM associated with EDX-ray diffraction detector (Thermo Fisher Scientific, Eindhoven, Netherlands). A TriStar II analyzer (Micromeritics, Norcross, GA, USA) was used for analyzing the textural properties of the sorbents. Prior to formal analysis, sorbent sample was swept under N_2 atmosphere for four hours at 130 °C. The S_{BET} (specific surface area, m^2/g) was deduced from N_2 sorption and desorption isotherms using the BET equation. The porosity (volume and pore size) was evaluated by the BJH method. For the study of the thermal degradation (TG-DTA) of sorbents, the samples were analyzed under N_2 atmosphere using a STA-449 F3-Jupiter thermoanalyzer (Netzsch, Gerätebau-HGmbh, Selb, Germany); the temperature ramp was set to 10 °C min^{-1}. FT-IR spectra were acquired using an IR-Tracer 100 FTIR spectrometer (Shimadzu, Tokyo, Japan) on dried samples pelletized (with KBr matrix). Sixty scans were collected for each sample analysis (with a resolution of 4 cm^{-1}). X-ray photoelectron microscopy was processed on the samples using an ESCALAB 250XI + instrument (Thermo Fischer Scientific, Inc., Waltham, MA, USA); the monochromatic Al K_α radiation was used (at 1486.6 eV energy; with a spot size of 500 μm; under a pressure of 10^{-8} mbar). The survey spectra were obtained for global identification of main elements, while the core-level spectra (with signal deconvolution) were collected after the calibration of binding energy (BE, eV) at 284.8 eV for $C_{adv.}$ signal. The pH-drift method was applied for the determination of the values of pH_{PZC} (pH of zero charge) [50]. A series of flasks filled with 0.1 M NaCl solutions at variable initial pH (pH_0, from 1 to 11) were mixed with the sorbents for

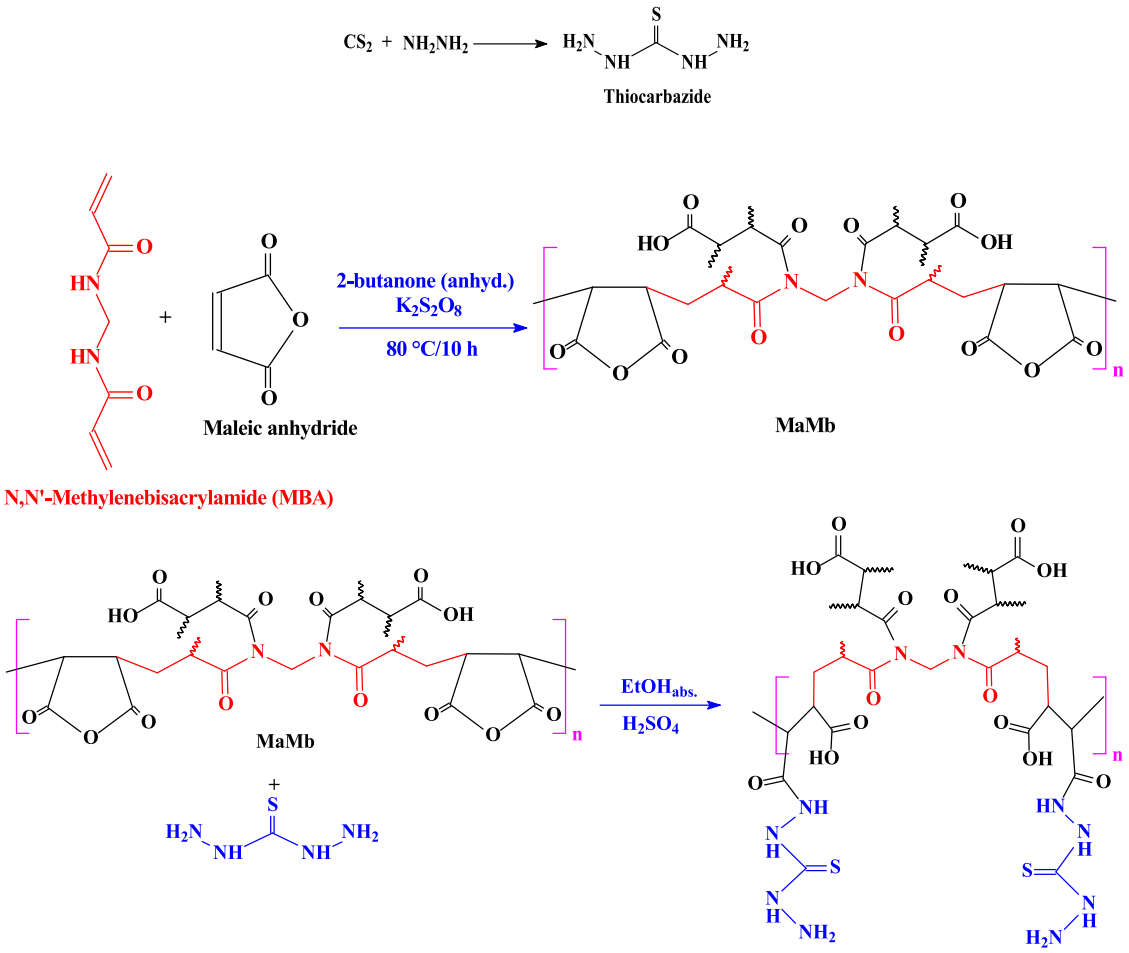

Scheme 1. Synthesis of MaMb and TcMaMb sorbents.

48 h; SD was set to 2 g L^{-1}. The final pH (i.e., pH_{eq}) was plotted against pH_0; pH_{PZC} corresponds to $pH_0 = pH_{eq}$. The pH of the solutions was measured using a S220-seven Compact pH-ionometer (Mettler-Toledo Instruments, Shanghai, China). Elemental analysis of sorbent samples were performed using a Vario-EL cube element analyzer (Elementar Analysensysteme GmbH-Langenselbold, Germany).

2.4. Sorption studies

Sorption studies were performed in batch systems. The stock solution was prepared with $Th(NO_3)_4$ salt at the concentration of 1 g L^{-1} (the pH was measured close to 4.22); working solutions were obtained by dilution into deionized water. The sorbent (m, g) was introduced under mixing (at v: 210 rpm) into a volume (V, L) of solution containing fixed concentration of metal ion (C_0, mmol Th L^{-1}). Unless specified, the sorbent dose (SD) was set to 0.66 g L^{-1}. Experimental conditions are systematically reported in the caption of the figures (see below). The standard temperature was 21 ± 1 °C; some experiments were also performed at T: 50 ± 1 °C for evaluating thermodynamic behavior. After fixed times (variable for the study of kinetics, after 48 h for equilibrium tests), a sample was collected from the reactor, filtrated (filter membrane pore size: ≈1 μm), and analyzed for residual concentration (C_{eq}, mmol Th L^{-1}) using ICP-AES (inductively coupled plasma - atomic emission spectrometry, ICP-7510 Shimadzu, Tokyo, Japan). The limit of detection was 0.9 μg L^{-1}, while the limit of quantification was 1 μg L^{-1}. The pH was not controlled during the sorption but it was systematically monitored at the end of the experiment. The sorption capacity (q_{eq}, mmol Th g^{-1}) was calculated from the mass balance equation (i.e., $q_{eq} = V\times (C_0 - C_{eq})/m$). The same procedure was used for testing the sorption properties from multi-component (equimolar) solutions. The distribution ratio (D, L g^{-1}) was defined using:

$$D = \frac{q_{eq}}{C_{eq}} \quad (1)$$

The selectivity coefficient of the sorbent for thorium against other metal ions ($SC_{Th/metal}$) is calculated from:

$$SC_{Th/metal} = \frac{D_{Th}}{D_{metal}} = \frac{q_{eq,Th} \times C_{eq,metal}}{C_{eq,Th} \times q_{eq,metal}} \quad (2)$$

Thorium desorption from metal-loaded sorbent was also operated in batch systems. Metal loaded-sorbents (q_{eq}, mmol Th g^{-1}) collected from the uptake kinetic experiments were mixed with the eluent (0.3 M HCl solution), using a SD close to 2 g L^{-1}. The concentration of the metal ion in the eluate was determined by ICP-AES and the desorption efficiency was calculated by mass balance (DE, %: $V_{eluent} \times C_{eluent} \times 100/(m \times q_{eq})$. A rinsing step (using demineralized water) was systematically applied between each sorption and desorption step.

Experiments were duplicated and the average values are presented (together with the standard deviation intervals in the relevant figures).

The modeling of experimental profiles in terms of kinetic experiments and sorption isotherms is processed through non-linear regression analysis, using the equations summarized in Tables S1 and S2.

2.5. Application to the treatment of ore leachate

The chemical constituents of the ore were determined after thermal acid digestion of the material (previously quartered) in 100 mL Teflon-beaker; the processing temperature was set to 150 °C, using different

acids: first, HF was used for silica mineralization, followed, after evaporation, by addition of HNO_3 and HCl (completed with H_2O_2 for organic material dissolution). After filtration, the volume of the solution was adjusted to 100 mL with demineralized water. Major and trace elements were analyzed in the solution using the following techniques. For uranium, the metal content was assessed by titration method using ammonium metavanadate [51,52], while the concentration of REEs was measured by the Arsenazo (III) method [53]. A UV-160 spectrophotometer (Shimadzu, Kyoto, Japan) was used for measuring the absorbance at the wavelength of 654 nm. The other elements were determined using Unicam-969 atomic absorption spectrometer (Thermo Electron Corporation, Waltham, MA, USA).

Several minerals were found in the ore (mainly constituted of aluminosilicate matrix), appearing as thorianite, thorite, and uranothorite (for uranium/thorium minerals), columbite (Fe-Nb mineral), zircon (zirconium silicate mineral), and xenotime (yttrium phosphate mineral). Most of these minerals need hard attack with either acid or base mineralization steps [3,54–56]. Hereafter, the ore sample underwent mild acidic leaching (in stirred tank): One kg of ore material was agitated with 3 L of 150 g L^{-1} H_2SO_4 solution for 3 h. The leachate produced from the leaching test was mixed with washing solution; the collected volume reached 2600 mL and the composition of the leachate is reported in Table S6. The leachate was pre-treated by sorption using a quaternary ammonium resin (25 g of Amberlite IRA400, ion-exchange resin, IEX resin in fixed-bed column: 0.5-cm diameter, 15-cm height). The pH of the leachate (2 L) was adjusted to 2, using $NaOH/H_2SO_4$ solutions. Based on the huge concentration of Fe(III) and Al(III) in the solution (which can interfere in the sorption process), the pH of the pre-treated leachate (outlet of IEX resin) was then adjusted to 4 and the residual concentrations were measured. This mild acid condition allows substantially precipitating Al(III) and Fe(III) with limited loss of other valuable metal ions. In the last step, the residual solution was tested for sorption at different pH values (in the range pH_0: 1–4) in the batch mode, using both MaMb and TcMaMb sorbents.

3. Results and discussion

3.1. Characterization of sorbents

3.1.1. Synthesis mechanisms

Metwally et al. [57] reviewed different methods applicable to the synthesis of thiocarbazide derivatives. In the case of the direct reaction of hydrazine hydrate with carbon disulfide, they showed that the total yield reached about 90 %. They also commented that thiocarbazide forms bidentate complexes (through S atom and amino group) with metal cations.

The amidation reaction of maleic anhydride with amine-bearing compounds was described by Ibrahim et al. [58]. Szkudlarek et al. [49] reported a series of reactions and modifications of maleic anhydride: they obtained a series of derivatives with alternating copolymer of 4-methyl-1-pentene and maleic anhydride (produced by free-radical polymerization mechanism at the –ene end-side). The same concept is used here for the synthesis of MaMb by the copolymerization of maleic anhydride with the ending groups of N,N'-methylenebisacrylamide. Szkudlarek et al. [49] described the amidoacidification derivative of maleic acid by reaction with 3-(dimethylamino)-1-propylamine: the primary amine reacts with the maleic cycle by cycle opening and grafting. The formation of TcMaMb proceeds through a mechanism similar to this amidoacidification reaction.

3.1.2. Physical characterization

The SEM micrographs show that MaMb and TcMaMb sorbents are irregular in both shape and morphology: both rounded particles and elongated structures can be observed (Fig. S1). Most of MaMb particles range between 20 and 30 μm, with irregular surfaces (~25 μm). In the case of TcMaMb, the size slightly decreases and ranges between 17 and 25 μm (~21 μm), while the particles show fluffy surfaces.

The textural characterization was performed by analysis of N_2 sorption and desorption isotherms (Fig. S2a,b). The application of the BET method shows that the specific surface area (S_{BET}) is comparable for MaMb (i.e., 56.75 m^2/g) and TcMaMb (i.e., 58.52 m^2/g). Their similar profiles are characterized by low adsorption over a long range of relative pressure (p/p_0 less than 0.8); this section is followed by a steep increase in adsorbed volume (almost vertical) up to p/p_0 0.98. The long initial plateau means that the multilayer adsorption is negligible (assimilated to Type Ib isotherm): this type of isotherm is observed for materials having broad range of wide micropores and narrow mesopores [59]. The second section can be identified as a Type IVa adsorption behavior. Generally, Type IV isotherm is assigned to mesoporous adsorbents with occurrence of condensation mechanisms; the presence of the hysteresis loop is associated with mesoporous wider than 4 nm and/or presence of conical and cylindrical mesopores with closed ends [59]. It is noteworthy that for the two sorbents and for both adsorption and desorption branches, a second wave is observed at $p/p_0 > 0.98$. This can be explained by analytical artifact or deformation. The analysis of the hysteresis loops shows for both MaMb and TcMaMab parallel sections for the adsorption and desorption branches. It is noteworthy that the hysteresis branches do not join; there is significant gap in the final plateau at $p/p_0 > 0.98$. This makes difficult the classification of the hysteresis loop. The parallel and almost vertical sections on the two branches are usually found in systems adopting H1 hysteresis loop. This characteristic has been assigned to narrow and uniform mesopores or networks of ink-bottle pores [59]. The application of the BJH method allows determining pore volume and pore size. The pore volumes are also comparable for MaMb and TcMaMb: 0.94 $cm^3\ g^{-1}$ and 1.03 $cm^3\ g^{-1}$, respectively. This is confirmed by the similarity in the pore sizes 667/449 Å and 725/486 Å, respectively; the first number corresponds to the determination based on the adsorption branch, the second on the desorption branch. These values are roughly consistent with the distribution of pore size appearing in Fig. S2c: the profiles are superposed for both MaMb and TcMaMb with pore sizes centered around 628 Å and 622 Å, respectively. The IUPAC ranks the pores according to micropore less than 2 nm < mesopore less than 50 nm < macropore. The sorbents are characterized by the coexistence of macro- and mesopores. The functionalization of the pristine sorbent hardly changes the textural properties of the material.

3.1.3. Chemical characterization

The thermogravimetric analysis of the sorbents is reported in Fig. S3. MaMb and TcMaMb TGA profiles are both characterized by four transitions in terms of weight loss.

(a) Below 159.5 °C (or 215.4 °C), the weight loss represents 10.1–13.9 %; this step corresponds to the release of water absorbed in the sorbents.
(b) In the range 159.5–310.1 °C (or 215.4–490.4 °C), MaMb loses 33.3 % and TcMaMb little more (around 42.6 %). This step corresponds to the degradation of ending groups (amine, carboxylic groups) and the depolymerization of the materials.
(c) In the range 310.1–560.7 °C (or 490.4–677.6 °C), the losses reach 26.5 % and 11.3 % for MaMb and TcMaMb, respectively. The carbonyl, carbamide and sulfone groups are degraded and the char begins to decompose.
(d) Above 560.7 °C (or 677.6 °C), the degradation of the chars represents 19.7 % and 5.5 % for MaMb and TcMaMb, respectively.

The total weight loss is significantly different for the two sorbents; the thermal stability is increased after functionalization. Indeed, weight loss reaches up to 89.6 % in the case of MaMb, while the functionalized material loses less than 73.4 %. Apparently, the grafting of thiocarbazide enhances the global stability of the sorbent. In the study of thermal degradation of metal-thiocarbazide complexes, Siddiqi et al. [60]

reported first the elimination of nitrogen-based compound at low temperature (below 170 °C), followed by a second transition associated with the degradation of organic backbone. The comparison of the DTG curves clearly shows that the functionalization changes the structure of the material (Fig. S4); this is evidenced by more intense peaks, the shifts toward higher temperatures (305.86 to 332.97 °C; 464.86 to 515.57 °C), and the appearance of a new peak at 583.97 °C. The weakly resolved shoulders at 654.66 °C and 680.62 °C in MaMb disappear after functionalization (being replaced by a plateau beginning at 737.77 °C).

The FTIR analysis of the sorbents (compared with thiocarbazide spectrum) allows following the synthesis of the sorbents (Fig. S5). Burns [61] reported a detailed analysis of FTIR spectrum of thiocarbazide. In the region 4000–2000 cm^{-1}, two groups of vibrations may be identified associated with: (a) $\nu_{O\text{-}H}$ ([62]) and $\nu_{N\text{-}H}$ (around 3300 cm^{-1}; [61]), and (b) $\nu_{C\text{-}H}$ aliphatic bonds (in the range 2950–2800 cm^{-1}). It is noteworthy that the contribution of the vibrations of N-based compounds in thiocarbazide (at 3125 and 3037 cm^{-1}) are observed at lower wavenumber than in MaMb (probably masked or altered by the presence of –OH groups). The spectrum of TcMaMb shows numerous bands coming from the convolution of the contributions of the vibrations of N-based and O-based functions. It is noteworthy that the grafting of thiocarbazide involves the appearance of a new band at 2713 cm^{-1}, which can be attributed to the opening of the maleic cycle and the interaction of carbonyl group with amine moiety of thiocarbazide (to form either an amide bond, an aminoacid-like, or an amine salt, [62]). Thiocarbazide shows the presence of two shoulders at 1769 and 1716 cm^{-1}, a band at 1678 cm^{-1}, and a shoulder at 1624 cm^{-1} (corresponding to $\nu_{N\text{-}H}$, [61]). In MaMb, the $\nu_{C=O}$ symmetric vibration is identified at 1703 cm^{-1}; this band is shifted toward 1664 cm^{-1} after grafting thiocarbazide (in TcMaMb). The sharp and intense band at 1597 cm^{-1} in MaMb, which is assigned to δ_{NH2}, is replaced by a broader band at 1597 cm^{-1}, (due to the grafting of new amine moieties, including secondary amine groups). The signal at 1410–1398 cm^{-1} is attributed to the bending vibration in carboxylic and aldehyde moieties in MaMb and TcMaMb (or sulfone moiety in thiocarbazide [63]). Rao and Venkataraghavan [64] also identified this band in several thiocarbonyl derivatives, where they assigned the signal to –N-C═S II band. The band at 1315–1313 cm^{-1} can be assigned to the presence of carboxylic groups in aminoacid-like environment [62]. Zhou et al. [48] identified the $\nu_{C=S}$ vibration at 1290 cm^{-1}. The broad band at 1195 cm^{-1} in thiocarbazide is attributed

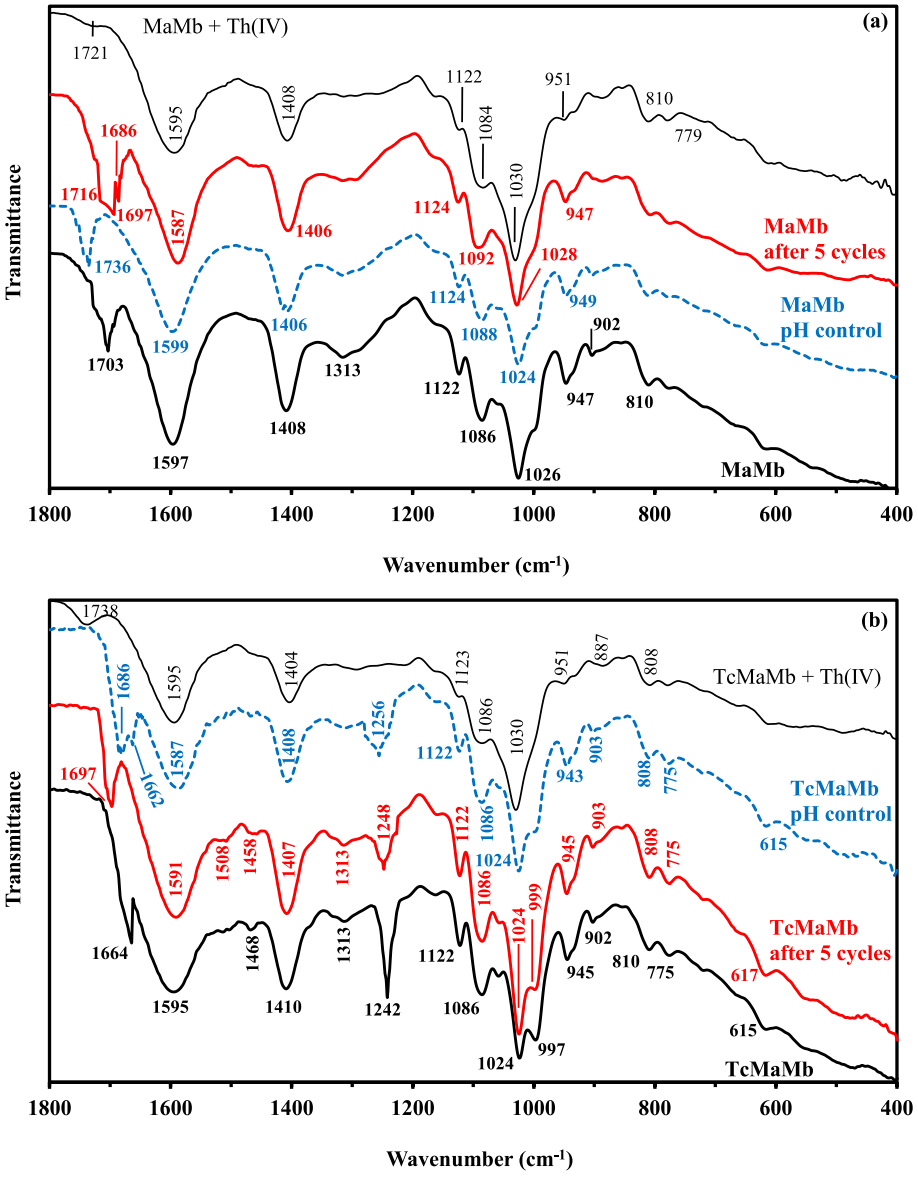

Fig. 1. Effect of environmental conditions (pristine, after conditioning at selected pH, after sorption of Th(IV), and after 5 cycles of sorption/desorption) on the FTIR spectra of MaMb (a) and TcMaMb (b) (wavenumber range: 1800–400 cm^{-1}).

to $\nu_{C=S}$ vibration; this band is shifted to 1242 cm^{-1} in TcMaMb [64]. In thiocarbazide, two bands at 1045 and 962 cm^{-1} can be observed, which can correspond to δ_{CNN}, or δ_{NCS} [61] or –N-C═S III band [64]. In the sorbents, a series of bands is observed at ≈1163 (shoulder), ≈1122, ≈1086, ≈1059 (weak), ≈1024, and ≈997 cm^{-1}; which correspond to contributions of $\nu_{NH,NH2}$, ρ_{NH2}, $\nu_{C\text{-}O}$, and δ_{OH} vibrations [65]. The strong band at 947–945 cm^{-1} and the small band at ≈902 cm^{-1} can be assigned to thiol ester vibrations (associated with tautomerization and reorganization of the "environment" of thiocarbonyl group) or internal carboxylic acid dimerization [62].

The FTIR spectra of the sorbents are compared at different stages of use, i.e., pristine sorbents, after being conditioned at the pH of thorium sorption, after thorium sorption, and after five cycles of sorption and desorption. The comparison of the spectra allows separating the possible effects of pH adjustment from the impact of metal binding. Fig. S6 shows that metal binding and pH control have limited effect on the spectra in the wavenumber range 4000–2000 cm^{-1}. The most significant changes are observed: (a) in the region where amine stretching vibration is identified (i.e., around 3200–3250 cm^{-1}) for both MaMb and TcMaMb, and (b) with the quasi disappearance of the band at 2729–2713 cm^{-1} in the case of TcMaMb. This means that N-based functional groups are involved in thorium binding with additional contribution of thiocarbonyl group in the case of TcMaMb sorbent. Fig. 1 compares the same spectra in the region 1800–400 cm^{-1}. In the case of MaMb sorbent, the band at 1703 cm^{-1} is significantly influenced by environmental conditions: with the pH control the band is shifted toward higher wavenumber (to 1736 cm^{-1}), while after thorium sorption the $\nu_{C=O}$ band almost disappears (appearing as a small shoulder at 1721 cm^{-1}). Another signal is specifically affected by thorium sorption: the band at 947 cm^{-1} is shifted to 951 cm^{-1} with a reduction in the relative intensity. Carboxylate groups are involved in thorium binding. In the case of TcMaMb, the band at 1664 cm^{-1} (i.e., $\nu_{C=O}$) is weakened (moving to 1662 cm^{-1}) while another stronger peak appears at 1686 cm^{-1} when controlling the pH to 4–4.5. This is associated with the protonation of some of these carboxylate groups. After metal sorption, the intensity of the band is strongly reduced and the wavenumber is even more shifted (up to 1738 cm^{-1}). Thorium binding also strongly affects the band at 1242 cm^{-1} (broadened and shifted to 1256 cm^{-1} after pH control): the $\nu_{C=S}$ vibration disappears with Th(IV) sorption. Consistently with MaMb sorbent, the band at 945 cm^{-1} is shifted to 951 cm^{-1} (with lower relative intensity) after metal uptake. Carboxylate and amine groups contribute to Th(IV) sorption onto the two sorbents; however, in the case of TcMaMb the thiocarbonyl group is also involved in metal sequestration. Zhou et al. [66] reported mixed contributions of functional groups such as carboxylic groups combined with hydroxyl, sulfonate, and amino groups in the binding of U(VI) and Th(IV) using $CaCl_2$-Kelp biomass. In the study of Th(IV) complexation with morpholinemethylurea and piperidinomethylthiourea, Sheikh et al. [67] reported that the metal forms bidentate coordination bonds with nitrogen and thiocarbonyl S ligands groups.

The comparison of the FTIR spectra of pristine sorbents with the spectra of re-used sorbents (5 cycles) shows that the alternated cycles of sorption and desorption do not significantly alter the chemical structure of the sorbents. The most significant variation in FTIR spectra is detected around the band at 1703 cm^{-1} for MaMb: the band is enlarged and shifted (to 1716–1697 cm^{-1}). In the case of TcMaMb, the band is shifted from 1664 cm^{-1} to 1697 cm^{-1}. Carboxylate groups are converted to carboxylic acid groups (due to the use of acidic solution for metal desorption and simple water rinsing between the re-use cycles). Apart this alteration of carboxylate groups, the spectra are poorly changed after five recycling steps. This clearly demonstrates the remarkable stability of the sorbents. This conclusion can be correlated with the limited loss in sorption and desorption properties at recycling, especially for TcMaMb (see Section 3.2.5.).

Fig. 2 compares the XPS survey curves for TcMaMb before and after Th(IV) sorption. The typical signals of C *1s*, O *1s*, N *1s*, and S *2p* are identified; the effective grafting of thiocarbazide is demonstrated by the presence of sulfur element. The weaker intensity of the S *2p* signals is directly correlated with the low level of sulfur content (notably compared with N content and the high density of N-based moieties in thiocarbazide, and with O content, highly present in maleic anhydride moiety, and their derived compounds). After thorium sorption, the markers of the metal appear, especially with the doublet Th $4f_{5/2}$ and Th $4f_{7/2}$ [68]. This is confirmed by the core-level spectra of selected signals for TcMaMb and Th-loaded TcMaMb (Figs. S7–S9). The deconvolution of the signals allows identifying the functional groups present on the sorbent: carboxylic group (C═O and C-OH bonds), the thiocarbonyl function (C═S and C—S bonds), the *N*-based bonds (primary, secondary amine groups, N—N links, N—C(=O or = S) bond). The C *1s* signal is poorly affected by metal binding. On the other hand, the deconvolution of O *1s* signal substantially changes after Th(IV) binding: the percentages of the different compounds evolve, while the BEs of C-OH signal is shifted toward lower value. Carboxylic group is involved in thorium sorption through O-Th bond. The signal N *1s* is poorly resolved making difficult the analysis and the determination of specific BEs. However, apparently after Th(IV) binding the deconvoluted signals are affected both in terms of BEs and atomic percentages (as appearing in Figs. S8 and S9); meaning that N-bearing functional groups contribute to metal sequestration. A new band appears at 395 eV, assigned to Th-N bond. It is noteworthy that the presence of nitrate is confirmed by the appearance of a new component at 407.4 eV. Table S3 summarizes the binding energies (BEs, eV) of deconvoluted components of selected signals and their atomic percentages. The global analysis of the changes in core-level spectra of selected signals confirms the binding of thorium through interactions with N-based, S-based and O-based ligands.

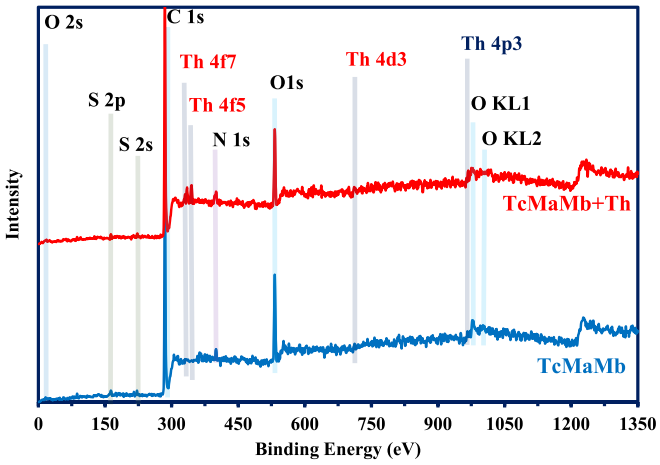

Fig. 2. XPS survey spectrum for TcMaMb sorbent before and after Th (IV) sorption.

The elemental analysis of the sorbents shows that, the grafting of thiocarbazide increases the nitrogen content (from 1.47 to 5.29 mmol N g^{-1}; i.e., variation of 3.82 mmol N g^{-1}) (Table S4). The effective grafting is also confirmed by the appearance of sulfur (0.68 mmol S g^{-1}): this amount is lower than expected from the molar ratio in thiocarbazide (i.e. N/S: 4/1). This means that the synthesis involves variations in the synthesis mechanism compared with theoretical profile. This is also demonstrated by the decrease in O content (from 28.40 to 26.80 mmol O g^{-1}).

The pH-drift method allows evaluating the pH_{PZC} values for MaMb and TcMaMb (Fig. S10). The pristine polymer bears acidic functions (resulting from the opening of the maleic anhydride ring) that lead to a pH_{PZC} value as low as 3.85. After grafting thiocarbazide, amino moieties bring alkaline functionalities (primary and secondary amine groups); therefore, the functionalization shifts pH_{PZC} to higher value (close to 5.25). The predicted value of pK_a for thiocarbazide is calculated to 10.58

± 0.70. This variation may be also affected by the tautomerization effect associated with thiocarbonyl group.

3.2. Sorption studies

3.2.1. Effect of pH

The pH may affect the sorption of metal ions through different effects such as the protonation/deprotonation of reactive groups on the sorbent, but also through the speciation of metal ions in the solutions (formation of hydrolyzed species, polynuclear species, depending on the metal ions and to the presence of soluble ligands). Fig. 3 compares the effect of the pH on the sorption of Th(IV) from low and high metal concentrations solutions (at C_0: 0.44 and 1.89 mmol Th L^{-1}, respectively), and at room temperature (i.e., 21 ± 1 °C) *vs* T: 50 ± 1 °C. The first conclusion of these tests concerns the beneficial effect of increasing the temperature: the sorption capacity systematically increases (regardless of the pH and the sorbent) with the temperature: the sorption is endothermic; this is specially marked in the case of MaMb. At the optimum pH, temperature increases sorption capacity by 50 % for MaMb and 25 % for TcMaMb. In addition, this figure clearly demonstrates the substantial increase in the sorption capacity after functionalization of pristine sorbent. Under comparable conditions, the sorption capacity at pH_{eq} 4.9 increases by 2.5-fold at T: 21 °C and 2.1-fold at T: 50 °C. Obviously, these preliminary tests justify the interest of this chemical modification.

The pH-edge curves follow the same trend: at low pH (i.e., pH ≈1), the sorption capacity remains between 0.049 and 0.126 mmol Th g^{-1}. Under these conditions, the reactive groups at the surface of the sorbents

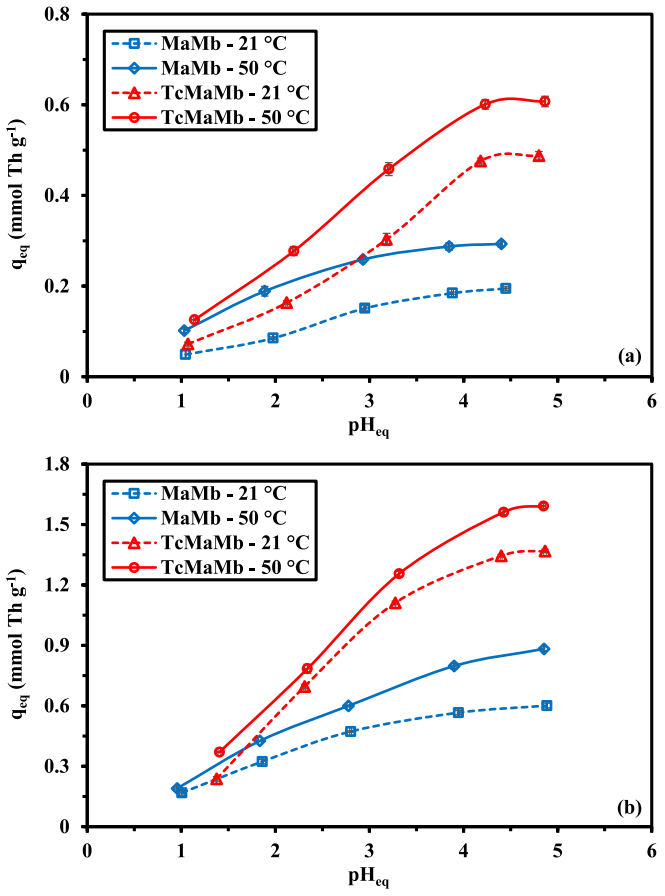

Fig. 3. Effect of pH on Th(IV) sorption using MaMb and TcMaMb sorbents – Effect of temperature and initial metal concentration: (a) C_0: 0.440 mmol Th L^{-1} and (b) C_0: 1.89 mmol Th L^{-1} (Sorbent dose, SD: 0.667 g L^{-1}; time: 48 h; T: 21 ± 1 °C; v: 210 rpm).

are protonated. The protons may act as strong competitor ions for metal binding onto the sorbents. Indeed, the speciation of thorium (nitrate) in aqueous solution is formed of cationic species as free Th^{4+} and hydroxocomplexes (such as $ThOH^{3+}$, $ThOH)_2^{2+}$, and $Th(OH)_3^+$) under acidic conditions, while at highest pH values neutral (and poorly soluble) species may appear as $Th(OH)_4$ [69,70]. With the increase in metal concentration and pH, polynuclear polyhydrolyzed species (bearing highly cationic charge) may be also formed [71]. This phenomenon may be completed by the formation of colloids and precipitates when pH significantly exceeds 4 [69,72]. When the pH increases, the competition effect decreases and the protonation progressively decreases. Therefore, sorption capacity increases with pH up to 4.5 (tending to stabilize above). With a pH_{PZC} value close to 3.85, MaMb sorbent becomes neutral or negatively charged at higher pH. In the case of TcMaMb, the surface remains globally positive in the totality of selected pH range (pH_{PZC}: 5.25). Despite the positively charged surface of the functionalized sorbent and the predominance of cationic metal species in the solution, the sorbent maintains high levels of recovery. Thorium may be bound onto carboxylate groups and amine groups (though chelation and possible ion exchange between protons onto amine groups and metal cations) for MaMb. It is noteworthy that in the pristine sorbent, tertiary amine groups are less favorable for metal binding due to steric hindrance and poor availability for metal chelation. In the case of TcMaMb, the introduction of thiocarbonyl groups brings additional sulfur reactive groups; besides, the chemical modification increases the N-content (coming from thiocarbazide), as secondary and primary (ending) amine groups (with higher reactivity than tertiary amine groups in MaMb). This was discussed and referred to relevant literature in Section 3.1.3.

Fig. S11 compares the pH variations for the different systems. The temperature does not influence the pH variation (in the range 21–50 °C). At low metal concentration (Fig. S11a), for pristine sorbent the pH is not changed up to pH_0 4, while above the pH tends to decrease (from 5 to 4.4). On the opposite hand, for TcMaMb the pH slightly increases by less than 0.3 pH unit (up to pH_0 4); at pH_0 5, the equilibrium pH slightly decreases (by 0.2 pH unit). When the concentration increases (up to 1.89 mmol Th L^{-1}), the pH variations are substantially increased, especially for TcMaMb (by 0.3–0.4 pH unit) (Fig. S11b). At pH_0 5, the equilibrium pH is almost unchanged for the two sorbents (less than 0.2 pH unit). The larger pH variations observed with TcMaMb can be directly correlated with the respective pH_{PZC} values of the sorbents: hence, the high pH_{PZC} value of TcMaMb induces larger pH variation.

Fig. S12 shows the effect of the pH on the distribution ratio ($\log_{10}$ plot). None of the curve shows a linear trend that could be related to the stoichiometric ion exchange ratio. At the optimum pH, the distribution ratio (L g^{-1}) reaches 1.45 ± 0.02 and 1.10 ± 0.05 for TcMaMb (at 50 °C and 21 °C, respectively); these values are >2-fold the levels reached for MaMb: 0.563 ± 0.003 and 0.342 ± 0.001, respectively. These values confirm the superior efficiency of TcMaMb for concentrating Th(IV).

For further studies, pH 4 was selected for optimal sorption and prevention of precipitation phenomena. This is consistent with the choice adopted by Albayari et al. [73] using biochar for thorium recovery from aqueous solutions. Humelnicu et al. [74] also reported optimum pH value close to 4 in the case of Th(IV) sorption onto amine-functionalized silica. Similar behavior was found for thorium removal using $CaCl_2$-modified Kelp biomass [66]. Orabi et al. [75] worked at pH 3 for Th(IV) sorption onto acrylic fiber-marine algae composite. In the case of phosphorodiamidate-functionalized silica, Zhang et al. [20] reported a higher efficiency for thorium removal at pH close to 2.5.

3.2.2. Uptake kinetics

The kinetics of Th(IV) sorption are compared for MaMb and TcMaMb in Fig. 4. The equilibrium is reached in 30 min in the case of the functionalized sorbent, while 120-180 min are necessary for the pristine sorbent. The textural characteristics of the two sorbents being very similar, this difference in equilibrium time is probably attributable to the proper reactivity and density of reactive groups rather than the

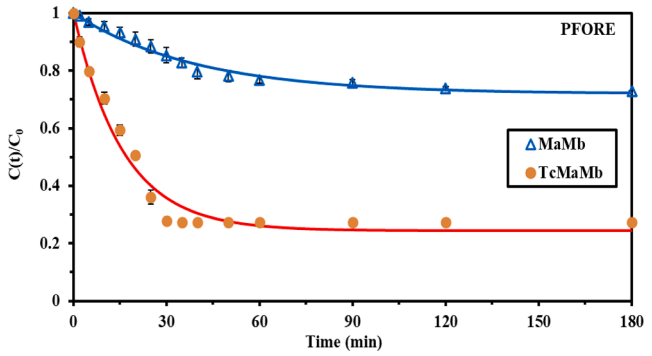

Fig. 4. Th(IV) uptake kinetics using MaMb and TcMaMb sorbents – Modeling of uptake kinetics using the pseudo-first order rate equation (pH_0: 4; C_0: 0.44 mmol Th L^{-1}; SD: 0.667 g L^{-1}; T: 21 ± 1 °C; v: 210 rpm).

diffusion constraints. As expected from the study of pH effect, the higher sorption capacities for modified sorbent allows decreasing drastically the value of relative equilibrium concentration. In addition, the functionalization significantly improves the initial slope of the curve. Hence, the $t_{50\%}$ (time required to achieve 50 % of sorption at equilibrium) decreases from 28 min for MaMb to 13 min for TcMaMb.

Uptake kinetics may be controlled by resistance to diffusion (including steps of bulk diffusion and film diffusion on one side, and intraparticle diffusion on the other side). Previous investigations showed that stirring speed of 200 rpm is sufficient to avoid the constraints of resistance to bulk diffusion and to limit the resistance to film diffusion (which is usually detected within the first minutes of contact). For these reasons, the discussion of kinetic profiles focuses on the effect of resistance to intraparticle diffusion (RIDE, hereafter simulated by the simplified approach described by the Crank equation, see Table S1) and to the proper reaction rates (approached through pseudo-first and pseudo-second order rate equations, PFORE and PSORE, Table S1). The PFORE and PSORE equations were initially developed for describing homogeneous chemical reactions before being extended to heterogeneous systems; therefore, the reaction rate coefficient must be considered as an apparent rate coefficient that integrates the proper contributions of mechanisms of resistance to diffusion. The PSORE is frequently associated to chemical sorption mechanism. However, Simonin [76] and Hubbe et al. [77] meaningfully discussed the misuse of this short-cut and they pointed out a series of requirements that generally are not appropriately fulfilled (leading to inappropriate interpretation). One of the most common error concerns the profile of concentration decay: the bulk concentration should be unchanged during the sorption step (which corresponds to the infinite volume mode). Here, the concentration decay (27 % and 73 %) is significant, making the interpretation inappropriate.

The application of the three models is compared for the two sorbents under comparable experimental conditions in Table 1. Both the determination coefficient (i.e.; R^2) and the Akaike Information Criterion (i.e.; AIC) show that the kinetic profiles are best fitted by the PFORE (>PSORE > RIDE). This is confirmed by the very close values of calculated sorption capacity at equilibrium (i.e., $q_{eq,1}$) with the experimental values of the equilibrium sorption capacities (i.e., $q_{eq,exp}$): the PFORE overestimates the experimental value by less than 4 %. In Fig. 4, the solid lines represent the fitting of kinetic profiles with the PFORE. The faster sorption (visually correlated with the initial slope of the decay curve) is confirmed by the values of the apparent rate coefficient (i.e., k_1): the functionalization of the sorbent increases k_1 value from 0.025 min^{-1} to 0.063 min^{-1}. These values are consistent with those reported by Abd El-Magied et al. [78] in the case of silica monoliths (i.e., k_1 ≈0.04 min^{-1}). In the case of functionalized silica (with phosphorodiamidate moieties), Zhang et al. [20] reported higher values ranging between 0.078 and 0.183 min^{-1} (depending on the derivatives).

Table 1
Parameters for the modeling of Th(IV) uptake kinetics.

Modeling			Sorbent	
Model	Parameter	Unit	MaMb	TcMaMb
Experimental	$q_{eq,exp.}$	mmol Th g^{-1}	0.199	0.532
PFORE	$q_{eq,1}$	mmol Th g^{-1}	0.205	0.553
	$k_1 \times 10^2$	min^{-1}	2.53	6.31
	R^2		0.981	0.976
	AIC		−124	−92
PSORE	$q_{eq,1}$	mmol Th g^{-1}	0.266	0.634
	$k_2 \times 10^2$	g $mmol^{-1}$ min^{-1}	8.62	12.7
	R^2		0.967	0.942
	AIC		−116	−79
RIDE	$D_e \times 10^{13}$	m^2 min^{-1}	6.78	6.85
	R^2		0.963	0.943
	AIC		−112	−77

Despite the lower efficacy of the RIDE (for fitting the experimental profiles, Fig. S13), the equation can be used to roughly evaluate the effective diffusion coefficient (i.e., D_e, m^2 min^{-1}) and to compare with the free diffusivity of Th(IV) in water (i.e., $D_0 = 3.19 \times 10^{-8}$ m^2 min^{-1}, [79]). The effective diffusivity is found close to 6.8×10^{-13} m^2 min^{-1} for the two sorbents. This is about five orders of magnitude lower than the free diffusivity of Th(IV) in water. This is a clear confirmation that the resistance to intraparticle diffusion contributes to the global control of uptake kinetics. This is consistent with the fact that despite the small size of sorbent particles (i.e., 25–21 μm) the required time for reaching the equilibrium ranges between 30 and 120 min (depending on the sorbent). The sorption is not simply restricted to the external surface but may also occurs in the bulk of the sorbent. Surprisingly, despite similar textural properties the equilibrium is reached faster for the functionalized sorbent (i.e., TcMaMb). However, the effective diffusivity coefficients are very close for the two materials: this apparent incoherence between the equilibrium times and the diffusivity coefficients is probably due to the crossed contributions of resistance to diffusion and proper reaction rate. Abdel Raouf and El-Kamash [80] reported a value close to 1.14×10^{-10} m^2 min^{-1} for the diffusivity coefficient of Th(IV) into TBP-impregnated sorbent. On the other hand, the effective diffusivity of Th(IV) into tridodecyl amine impregnated Amberlite XAD4 was found close to 5.46×10^{-17} m^2 min^{-1} [81].

3.2.3. *Sorption isotherms*

The beneficial effect of sorbent functionalization is also illustrated by the comparison of sorption isotherms (Fig. 5). Both the maximum sorption capacity (at sorbent saturation) and the initial slope are strongly increased. The profiles are substantially different for the two sorbents: the sorption capacity plotted *vs* equilibrium concentration strongly increases in the low concentration range for TcMaMb, while for pristine sorbent the increase in sorption capacity is more progressive. The $C_{eq,50\%}$ (residual concentration corresponding to the half maximum sorption capacity) decreases from 0.487 mmol Th L^{-1} for MaMb to 0.176 mmol Th L^{-1} for TcMaMb. The initial slope is directly correlated with the affinity of the sorbent for the solute. Several models were tested for the simulation of sorption isotherms (see Table S2). Three of these models retain more attention based on selected statistical criteria (Table 2). In the case of MaMb, the exponential shape of the sorption isotherm can be better correlated with the Freundlich equation (Fig. S14). This empirical equation is usually associated with multi-layer sorption with interactions between sorbed molecules and heterogeneous distribution of sorption energies. This profile is also frequently encountered when the investigated range of concentration is not large enough to reach the saturation of the sorbent (appearing as a plateau); this is probably the case here. Increasing the concentration range would be meaningless in terms of application: the concentration effect would be too low for

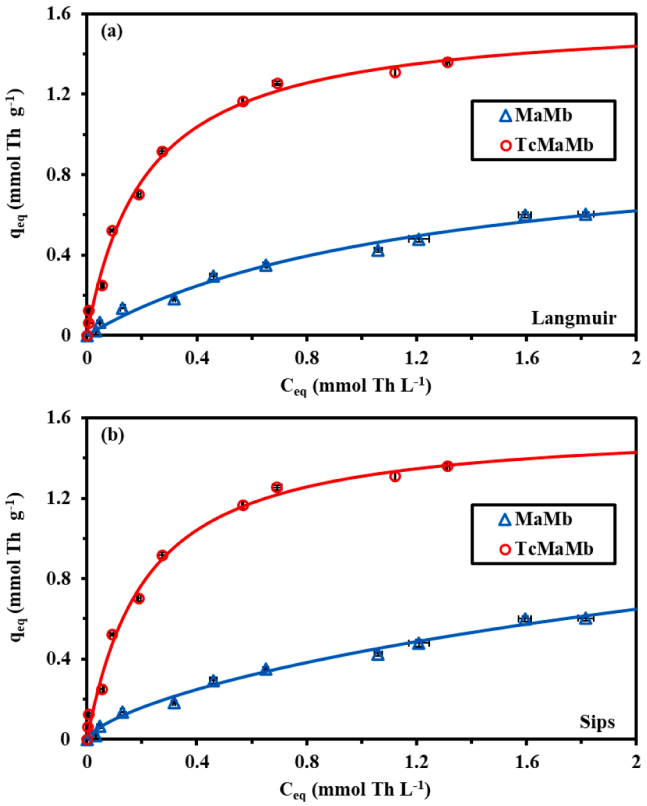

Fig. 5. Th(IV) sorption isotherm using MaMb and TcMaMb sorbents – Modeling of uptake kinetics using the Langmuir equation (a) and the Sips equation (b) (pH_0: 4; C_0: 0.047–2.2 mmol Th L^{-1}; SD: 0.667 g L^{-1}; T: 21 ± 1 °C; v: 210 rpm).

Table 2
Parameters for the modeling of Th(IV) sorption isotherms.

Modeling			Sorbent	
Model	Parameter	Unit	MaMb	TcMaMb
Experimental	$q_{m,exp.}$	mmol Th g^{-1}	0.603	1.359
Langmuir	$q_{m,L}$	mmol Th g^{-1}	1.008	1.593
	b_L	L $mmol^{-1}$	0.809	4.646
	R^2	–	0.988	0.994
	AIC	–	−76	−65
Freundlich	k_F	$mmol^{1-1/nF}$ $L^{1/nF}$ g^{-1}	0.431	1.321
	n	–	1.627	2.510
	R^2	–	0.991	0.966
	AIC	–	−80	−46
Sips	$q_{m,S}$	mmol Th g^{-1}	2.82	1.563
	b_S	$L^{1/nS}$ $mmol^{-1/nS}$	0.183	5.180
	n_S	–	1.42	0.962
	R^2	–	0.991	0.994
	AIC	–	−77	−61

making applicable the sorption process. The Langmuir equation is associated with monolayer sorption without interactions between sorbed molecules and with homogeneous sorption sites (equivalent sorption energies). The asymptotic trend of this equation is more appropriate to describe Th(IV) sorption isotherm for TcMaMb: this is confirmed by the values of statistical criteria. The Sips equation gives comparable fitting of MaMb isotherm than the Langmuir equation (though less than Freundlich equation). The Sips equation combines the Langmuir and the Freundlich equations; the third-adjustable parameter may help in mathematically fitting experimental profiles (at the expense of a loss in mechanism interpretation). The AIC statistical parameter allows reducing this effect in the evaluation of fitting since it takes into account the number of adjustable parameters. It is noteworthy that the calculated sorption capacity at saturation of the monolayer (i.e., $q_{eq,L}$, in the Langmuir equation) significantly overestimates the experimental value by 17 % for TcMaMb; the poor fitting of MaMb profile by the Langmuir equation is reflected by the poorly representative value of $q_{eq,L}$ (i.e., 1.008 *vs* 0.603 mmol Th g^{-1}). This overestimation is directly explained by the fact that the saturation plateau is not reached.

The maximum sorption capacity is significantly increased by functionalization: the $q_{m,exp}$ for TcMaMb is 2.25-fold the value for pristine sorbent. The increase in the density of sorption sites (especially S-based and N-based moieties) can explain this enhancement. However, this increase is not directly proportional to the increase in N content (from 1.47 to 5.29 mmol N g^{-1}) nor the appearance of S-bearing group (i.e., 0.68 mmol S g^{-1}). This can probably be explained by the existence of chemical sites that are not reactive (or be sterically hindered) and by the contribution of different functional groups in the sorbent for the binding of thorium cations (to fulfill the coordination mode of the metal).

Table S5 reports Th(IV) sorption properties for a series of alternative sorbents. Atta et al. [29] synthesized a highly efficient sorbent (rosin amidoximed capped magnetite nanoparticles): they found for this outstanding material a maximum sorption capacity close to 2.46 mmol Th g^{-1} (at pH 4). The affinity coefficient was in the same order of magnitude of the value reported for TcMaMb, while requesting a higher contact time for reaching the equilibrium. The maximum sorption capacity of MaMb is comparable to many of these sorbents such as functionalized chitosan magnetite-chitosan composite [82], macroporous polyacrylamide-based monolith [83], mesoporous graphite carbon nitride [84], or DETA/GMA/cellulose composite [85]; the affinity coefficient for MaMb is significantly lower than the values reported for these alternative sorbents. The functionalization of the pristine sorbent substantially increases the sorption standards of the sorbent to reach performances comparable to those of the most efficient materials such as magnetic TiO_2/GO nanocomposite [22], graphene/TiO_2 [86], or thiourea-modified/SiO_2 composite [13]. Globally, the combined properties of TcMaMb allows classifying this sorbent as one of the most efficient sorbents for thorium recovery from aqueous solutions.

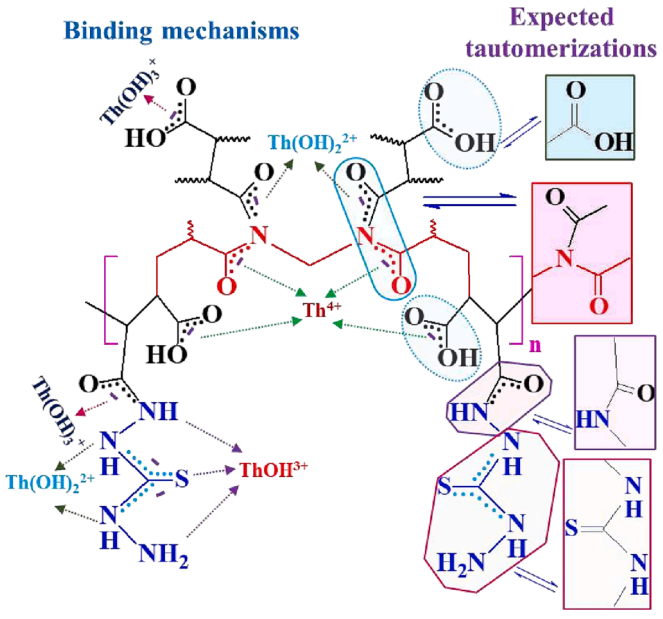

Scheme 2. Tentative mechanisms for Th(IV) sorption onto TcMaMb (potential effects of tautomerization on reactive groups).

3.2.4. Sorption mechanism

Scheme 2 reports the different mechanisms that can be involved in the binding of Th(IV) onto TcMaMb (and MaMb). These mechanisms depend on the pH and the pH_{PZC} values (meaning protonation/deprotonation of reactive groups and tautomerization effects). The overall charge of the sorbent affects the attraction/repulsion of specific metal species (Th^{4+}, $Th(OH)^{3+}$, $Th(OH)_2^{2+}$, $Th(OH)_3^{+}$, including polynuclear hydrolyzed species at high pH and concentration values, [87]) through electrostatic attraction or ion exchange but also the possibility to chelate these species (depending on charge compatibility, and charge repulsion effects). The tautomerization effects contribute to the delocalization of bonds [88] and the modification of local electronegativity; which in, turn, influences their reactivity through complexation. These combined effects make complex the interpretation of binding mechanisms. However, the most probable modes of binding can be reported as:

(a) electrostatic attraction of positively charged metal ions (metal speciation, [69,71,72]) onto partially protonated functional groups (linked with pH values against pH_{PZC}), and.

(b) chelation properties involving deprotonated functional groups (conditioned by tautomerization of partially negatively-charged groups and π bonds) and free Th^{4+} (or hydrolyzed forms).

For supporting these hypotheses, FTIR analyses confirmed the contribution of –NH, –OH, C═S and C═O groups: the modification of their chemical environment is shown by the decrease in their relative intensity, and/or the shift of their wavenumber. Multidentate complexes may be formed as it occurs directly with thiocarbazide and derivatives [57,60], meaning that several functional groups are simultaneously involved in metal binding. This is even favored by the tautomerization effect of the reactive groups. Some of these interpretations at the molecular level (especially for C═O and –NH groups) are also confirmed by XPS analysis. At the macromolecular level, the effect of the pH on the sorption confirms the importance of favoring both the deprotonation and the tautomerization effects (meaning chelation mechanisms) by pH increase up to 4–4.5. Above this pH value, the sorption capacity tends to stabilize. Increasing the pH above 4 favors first the formation of hydrolyzed species (including polynuclear forms) and the formation of colloids and precipitates, especially at high metal concentration (inducing the overestimation of sorption performance).

3.2.5. Metal desorption and sorbent recycling

When using waste materials (such as biosorbents), the minimal cost of the material makes possible the single use of the sorbent; meaning the sorbent does not require to be reused. However, with chemical modification of the material or when using sophisticated method of synthesis, the recycling of the sorbent becomes a critical parameter for the global evaluation of the potential of the material. Hereafter, Th(IV) elution is compared for the two sorbents in terms of both desorption kinetics (Fig. S15) and recycling efficiency (Table 3).

The high sensitivity of the sorbents to pH for the sorption of thorium opens possibility for metal elution playing with the pH. Though some studies reported the use of EDTA [74], or alcohol [89] for the elution of Th(IV), acidic solutions are generally preferred. Anirudhan et al. [90] tested a series of alkaline, and acidic solutions as well as salt solutions for Th(IV) desorption from metal-loaded PMA/chitosan/bentonite composite: they concluded on the superiority of 0.1 M HNO_3 solution. Although nitric acid solutions (0.1 M) have frequently been used [78,91], Cheira [19] preferred using 0.1 M HCl solution in the case of Th (IV) desorption from sulfonamide/silica composite. Many studies have already reported the use of nitric acid for desorption of thorium from metal-loaded sorbents. Yuan et al. [18] used 0.2 M HCl solution for successful and complete elution of Th(IV) from bi-functionalized mesoporous silica; however, even with a concentration of 0.02 M, the desorption yield reached 94 %. Tuzen et al. [22] suggested using 0.75 M HCl solutions (or higher concentrations) for thorium release from carbon nanofiber/polymer composite: desorption efficiency increased from 55 % to 87 %, and 98 % when concentration increased from 0.25 M to 0.75 M, and 1 M, respectively. Saleh et al. [92] used stronger acidic conditions (i.e., 1 M HCl solution was necessary for achieving 96 % yield) for thorium elution from bentonite-arabic gum composite. Hereafter, 0.3 M HCl solution was used for investigating the desorption kinetics (Fig. S15). The complete desorption of thorium is achieved in 30 min, regardless of the sorbent. It is noteworthy that the curves for MaMb and TcMaMb are superposed. The acidic solution displaces the speciation of thorium toward the formation of free thorium species (i.e., Th^{4+}); lower ionic size (compared with hydrolyzed species or polynuclear species at higher pH value) makes easier the diffusion of metal ions during the elution step.

Table 3 shows that the complete desorption of thorium is not affected by the recycling of the sorbent. On the other hand, the sorption efficiency tends to decrease with the number of cycles. However, the evolutions are different for the two sorbents. Indeed, while for MaMb the progressive decrease in sorption performance reaches 7.8 % at the fifth cycle (compared with initial sorption step); the loss in sorption efficiency does not exceed 1.8 % for the functionalized sorbent. The loss in sorption/desorption pattern is apparently more favorable than those reported by Saleh et al.[92] and Tuzen et al. [22], who reported decreases in performances higher than 10–15 % at the fifth cycle. This stability in sorption performances is consistent with the chemical stability of the sorbent after the fifth recycling, as characterized by FTIR analysis (Section 3.1.3.).

TcMaMb shows outstanding stability compared with pristine sorbent. The functionalization not only improves sorption performance (kinetics and sorption capacities) but also the life cycle (aging in recycling). Another important criterion for evaluating the potential of this material concerns the impact of the presence of competitor ions and the complexity of the solution. This question is addressed in the following sections through the evaluation of sorption selectivity from multi-component equimolar synthetic solutions (Section 3.2.6) and from real industrial solutions (obtained from the treatment of ore leachate, Section 3.3.).

Table 3
Recycling of MaMb and TcMaMb sorbents – Sorption and desorption efficiencies (SE and DE, %) for five successive cycles.

Sorbent	MaMb		TcMaMb	
Cycle	SE	DE	SE	DE
1	26.5 ± 0.1	100.1 ± 0.2	72.0 ± 0.0	100.2 ± 0.6
2	26.0 ± 0.8	100.0 ± 1.4	71.8 ± 0.2	99.9 ± 0.7
3	25.5 ± 0.9	99.8 ± 0.6	71.7 ± 0.1	99.5 ± 0.7
4	24.9 ± 0.6	100.0 ± 0.2	71.0 ± 0.7	100.2 ± 0.3
5	24.4 ± 0.8	100 ± 0.1	70.7 ± 0.6	100.2 ± 0.1
Loss at fifth cycle	7.8 %	Negligible	1.8 %	Negligible

3.2.6. Sorption selectivity

The sorption of thorium from multi-component solutions (at equimolar 1 mmol L^{-1} concentrations) at different pH values is reported in Fig. 6. Competitor elements are selected in relation with their usual presence in ore leachate. Herein, the term metal is extended to the case of silica metalloid. The selectivity coefficient (i.e., $SC_{Th/metal}$) was defined in Eq. (2). SC > 1 means the sorbent preferentially sorbs Th(IV) than competitor metal, and reciprocal. The comparison of the two panels in Fig. 6 clearly illustrates that the functionalization of MaMb strongly affects the selectivity for Th(IV) sorption. In the case of MaMb (Fig. 6a), the pH has a limited impact on metal sorption and selectivity. The $SC_{Th/metal}$ varies between 0.457 (for U(VI) at pH_{eq} 1.97, weak preference for uranyl ions) and 2.34 (for Al(III) at pH_{eq} 0.98, stronger affinity for Th (IV) against aluminum). It is noteworthy that under these acidic conditions, the sorption capacity of target metals is very low; for example, the cumulative sorption capacity at pH_{eq} 0.98 does not exceed 0.304 mmol g^{-1}; this relativizes the interest of applying this pH condition for metal separation. These values, while indicating a low preference for

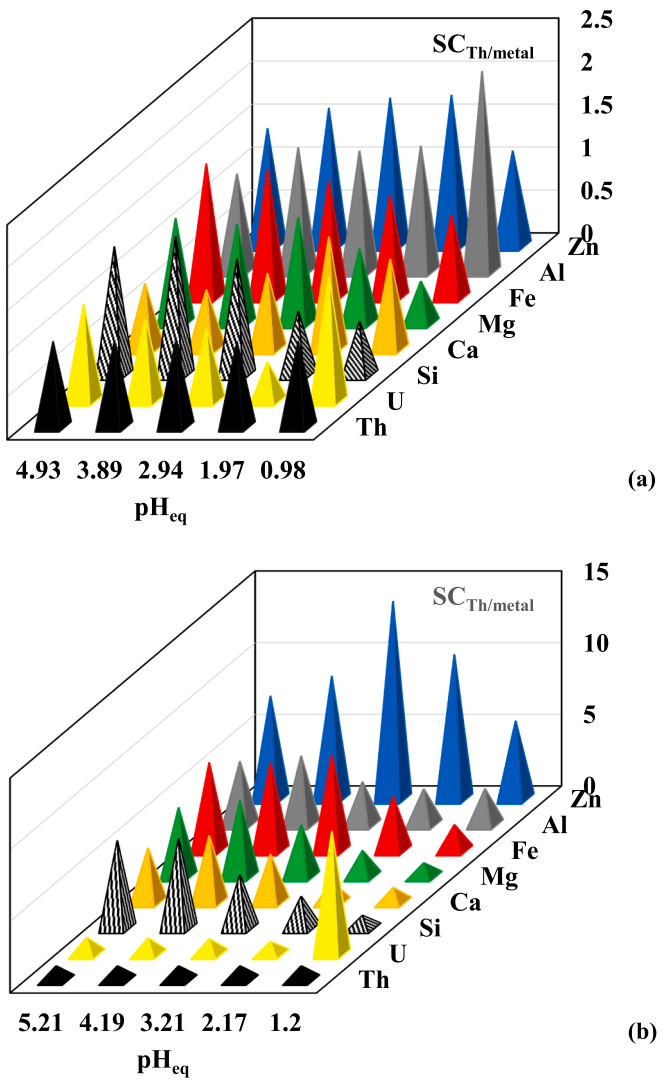

Fig. 6. Effect of pH on the selectivity coefficient ($SC_{Th/metal}$) for MaMb (a) and TcMaMb (b) sorbents (equimolar multi-component solutions, C_0: 1 mmol L^{-1}; SD: 0.667 g L^{-1}; v: 210 rpm; time: 24 h; T: 21 ± 1 °C; $SC_{Th/Th} = 1$ as reference).

specific metals, are insufficient to allow the selective separation of thorium from other metal ions. At pH_{eq} 4.93, the cumulative sorption capacity reaches 1.4 mmol g^{-1}; this is much higher than the maximum sorption capacity reached for Th(IV) in single-component solutions. This may be explained by two reasons: (a) the sorption of competitor metal ions onto other functional groups, and/or (b) the higher cumulative metal concentration that allows reaching the saturation of the sorbent (probably not reached in Fig. 5).

Fig. 6b shows a fully different pattern in the case of TcMaMb. First, the pH plays a significant role in the selectivity for Th(IV) recovery: best separation is obtained at pH_{eq} 4.19 and 5.21 (except against Zn(II), in which the greatest selectivity is achieved at pH_{eq} 3.21). Another figure deserves attention: while in general $SC_{Th/U}$ is close to 1, at pH_{eq} 1.2, the selectivity increases up to 8.6. It is noteworthy that under favorable conditions (pH_{eq} > 4) the sorbent shows high selectivity for Th(IV) against metalloid (Si(IV)), alkali-earth and base metals: $SC_{Th/metal}$ varies between 4.7 and 13.8. The functionalization of MaMb strongly enhances the selectivity of TcMaMb for Th(IV) against these elements, but not against U(VI). The grafting of thiocarbazide onto MaMb favors the preferential sorption of these two actinides against competitor elements. The maximum sorption capacity for Th(IV) reaches 0.42 mmol Th g^{-1}; this is more than two times lower than the value reached for Th(IV) sorption from mono-component solution (i.e., 0.98 mmol Th g^{-1}) at pH 4. The presence of competitor elements depreciates significantly the sorption of Th(IV) despite the selectivity of the sorbent for Th(IV). The maximum cumulative sorption capacity reaches 1.61–1.73 mmol g^{-1} at pH_{eq} 4.19–5.21. This value is higher than the maximum sorption capacity reached with Th(IV) single-component isotherm (i.e., 1.36 mmol Th g^{-1}): the other metal ions compete with the reactive groups responsible of Th(IV) sorption but can be also bound onto other functional groups. The selectivity of TcMaMb for Th(IV) against competitor elements can be ranked according to:

Ca ≈ Al ≈ Mg < Si < Fe ≪ U ≪ Zn (maximum value at individual optimal pH value).

More specifically, at pH_{eq} 4.19, the selectivity coefficients obey the sequence:

U (1.18) ≪ Ca (4.69) ≈ Al (4.82) ≈ Mg (5.33) < Fe (6.17) ≈ Si (6.28) ≪ Zn (8.60).

The radius (Å) of hydrated species follows the series [93]:

Th (1.13) > U (1.08) > Ca (1) > Zn (0.75) > Mg (0.71) > Fe (0.65) > Al (0.53).

It is not possible correlating the SC values with the ranking of the radius of hydrated metal species: there is a clear inversion between Al (III) and Zn(II) ranks, without any specific reason (though zinc is recognized for having in the Irving-Williams series a different pattern that the divalent first-row transition metals follow). Nieboer and Richardson [94] ranked Th(IV) and U(VI) within class A elements (together with Ca(II), Mg(II) and Al(III)), while Fe(III) and Zn(II) are borderline elements. Class A elements are seeking for oxygen-bearing ligands contrary to Class B elements (with higher affinity for N- and S-ligands). Borderline elements have intermediate behavior. In TcMaMb, the grafting of thiocarbazide brings additional sulfur-ligand and increases the density of N-ligands; both functional groups being more favorable to Class B elements (and by extension to borderline compared with Class A elements). Actually, according to HSAB principle [95], these new functional groups are not expected to increase the selectivity since they can have good affinity of some of these competitor metals. This means that other mechanisms may modulate this effect in relation with the steric arrangement of reactive groups and/or pH effect (and the relevant contributions of ion exchange and chelation mechanisms).

Fig. S16 provides another visualization of the preference of TcMaMb for Th(IV) and U(VI). The plot of the distribution ratio (i.e., D, L g^{-1}) for the different elements at the different pH values confirms that MaMb is poorly selective for the two actinides. The distribution ratio varies between 0.158 and 0.321 L g^{-1} for the pristine sorbent. On the opposite hand, for TcMaMb low distribution ratios are reported for Si(IV), Ca(II), Mg(II), Fe(III), Al(III) and Zn(II) (below 0.24 L/g). This is much lower than the value reported for U(VI) (tripled to 0.744 L g^{-1}); for Th(IV), the distribution ratio is even higher under the most favorable conditions (up to 0.88 L g^{-1}; i.e., 3.7-fold). Fig. S17 shows the evolution of enhancement of distribution ratio (at the different pH values) induced by thiocarbazide grafting: more pronounced effects on Th(IV) and U(VI) occur at pH_0 4–5.

All other conditions equal, it is possible to compare the sorption capacities for the two sorbents and to calculate the enhancement factor (β = q(TcMaMb)/q(MaMb)) for the different metals and different pH values (Fig. 7). This criterion shows that for most of the elements the functionalization does not improve the sorption capacity, and even decreases the affinity of the sorbent for metal ions such as Zn(II) (regardless of the pH, β less than 0.74), Fe(III) (β: 0.57–0.92), Mg(II) (β: 0.67–0.92), and Si(IV) metalloid (β: 0.64–0.98). For some metal ions, the enhancement factor depends on the pH, with little improvement; for example Ca(II) (enhancement decreases with increasing the pH). In the case of Al(III), the enhancement factor is negligible (varying between 0.93 and 1.21). Clearly, the functionalization significantly profits to U (VI) and Th(IV): β parameter increases with the pH, reaching a maximum at pH_0 4–5, where the sorption capacity increases by 2.3–2.5-fold with the grafting of thiocarbazide. It is noteworthy that this

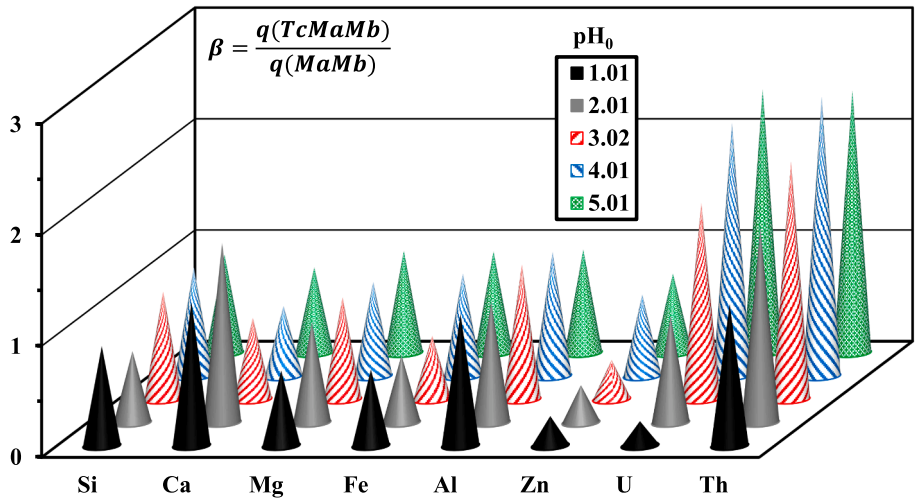

Fig. 7. Enhancement factor (β = q(TcMaMb)/q(MaMb)) for the multi-component equimolar solutions (C_0: 1 mmol/L; SD: 0.667 g/L; v: 210 rpm; time: 24 h; T: 21 ± 1 °C).

beneficial effect increases with the pH. At pH_0 4–5 the β-values follow the trend:

Th(IV)≈U(VI) [2.3–2.5] > Al(III),Si(IV),Fe(III) [0.88–1.12] > Ca(II), Zn(II) [0.63–0.77].

It is not possible finding a clear correlation between the ranking and the conventional criteria elaborated by Nieboer and Richardson [94] (i.e., Ionic Index as z^2 / r or covalent Index as $X_m^2 \times r$, where z is the formal charge of the metal ion, r the ionic (hydrated) radius, and X_m the Pauling electronegativity).

In the study of metal permeation through supported trioctylphosphine oxide membranes, Kedari et al. [96] showed that the system is selective for U(VI) and Th(IV) against a series of elements such as Al, B, Be, Ca, Cd, Cu, Fe, Mg, Mn, Ni, Pb, Si, Ti, and Zn (with a partial permeability of Zr). Yuan et al. [18] reported the selectivity of bifunctionalized silica (bearing phosphonate-amino groups) for thorium against Zn, Pb, Co, Ni, Sr, Cr(III), La, Ce, Cs, and Eu at pH 3.5. Ang et al. compared the selectivity of ion exchange resins [9] and chelating resins [10] for the separation of U(VI) and Th(IV) from lanthanides. The selectivity strongly depended on the pH. For iminodiacetic chelating resins, the pH profiles for uranium and thorium are superposed and more efficient because of the greater tendency of actinides to displace the protons from the carboxylic groups held by these resins compared with lanthanides [10]. In the case of aminophosphonic and picollylamine resins, the separation was not effective. In the case of strong and weak cation exchange, U(VI) and Th(IV) could not be separated from REEs contrary to strong base quaternary amine resins [9].

This study shows another singular advantage of TcMaMb; in addition, to the other benefits in terms of thorium sorption (capacity and kinetics), the functionalization of pristine MaMb strongly increases the selectivity of the sorbent for the two actinides considered in this section, with little preference for Th(IV) over U(VI).

3.3. Application to the treatment of ore leachate

3.3.1. Leaching and pre-treatment

Table S6 shows that selected leaching conditions allow recovering about 43 % of Th(IV) and 63 % of U(VI); relevant concentrations range between 131 mg Th L^{-1} and 241 mg U L^{-1} (i.e., 0.567 mmol Th L^{-1} and 1.01 mmol U L^{-1}). Iron(III) and Na(I) are also highly recovered from ore matrix (around 50 % leaching efficiency), with concentrations reaching values as high as 2.94 g Fe L^{-1} and 4.94 g Na L^{-1}; despite a lower leaching rate (i.e., 27 %) aluminum reaches up to 10.3 g Al L^{-1}. Other major elements are less released though potassium concentration may reach up to 1.73 g K L^{-1}. It is noteworthy that Si is negligibly leached from the ore (despite a content exceeding 68 %, in mass in the ore).

Amberlite IRA400 is an ion-exchange resin well known for its affinity for U(VI); this quaternary ammonium resin is commercially exploited for uranium recovery from acidic leachate. The pH of the solution was fixed at 2 to avoid excessive competition effect of Fe(III) and HSO_4^- in the removal of U(VI) [97], and maintain protonation of quaternary ammonium groups (favorable to U(VI) sorption). Table S7 confirms the good sorption of U(VI) (up to 85.7 %; residual concentration limited to 34.5 mg U L^{-1}), while thorium is marginally extracted from the solution (the loss does not exceed 9.5 %). Iron loss during the sorption step onto Amberlite IRA 400 remains close to 25 % (with a residual concentration as high as 2.19 g Fe L^{-1}), while the sorption removed less than 19 % of the other elements (only 4 % of Al(III)). The residual solution still contains huge concentrations of Fe(III) (i.e., 2.19 g Fe L^{-1}), Al(III) (i.e., 9.88 g Al L^{-1}), Na(I) (i.e., 4.19 g Na L^{-1}), and K(I) (i.e., 1.43 g K L^{-1}). These levels of concentration of Fe(III) and Al(III) may have a strong impact on the recovery of Th(IV) because of their huge excess. Metal/Th molar ratios exceed 713 for Al(III), 76 for Fe(III) (in addition to 354 for Na(I), 71 for K(I) and 18 for Ca(II) and Mg(II)). To minimize this competition effect, the residue of sorption onto Amberlite IRA 400 was pH-controlled to 4 (Table S8). This step allows removing most of Al(III) (about 86.6 %) and Fe(III) (around 91 %), with loosing less than 21 % of thorium and 26.4 % of uranium: the residual concentrations of Th(IV) and U(VI) reach up to 94.5 mg Th L^{-1} (i.e., 0.407 mmol Th L^{-1}) and 25.4 mg U L^{-1} (i.e., 0.107 mmol U L^{-1}). The molar excess of Fe(III) and Al(III) are reduced to 8.6-fold and 121-fold, respectively. These levels of competitor ions become more acceptable for the application of the sorption process onto MaMb and TcMaMb sorbents.

3.3.2. Sorption tests

The comparison of sorption performances for the different elements is made difficult in the case of pre-treated leachate because of the huge excess of some of these metal ions (such as Al(III), Fe(III) of Na(I)). For this reason, it sounds more interesting focusing on the comparison of binding criteria between pristine MaMb and TcMaMb. In Fig. 8, the change of scale between the two panels confirms that the grafting of thiocarbazide significantly enhances the preference of the sorbent for Th (IV) (preferentially to U(VI), in Fig. S18; the two metals show the same trend). The improvement in the SC values increases consistently with the pH, while for MaMb the pH effect is less pronounced. Another indicator allows measuring the beneficial effect of the functionalization in the treatment of ore leachate (Fig. S19): the distribution ratio (i.e., D) reaches 2.29 L g^{-1} for Th(IV) and 1.10 L g^{-1} for U(VI), under the most favorable conditions (i.e., pH_{eq}: 4.22), while for the other elements the D

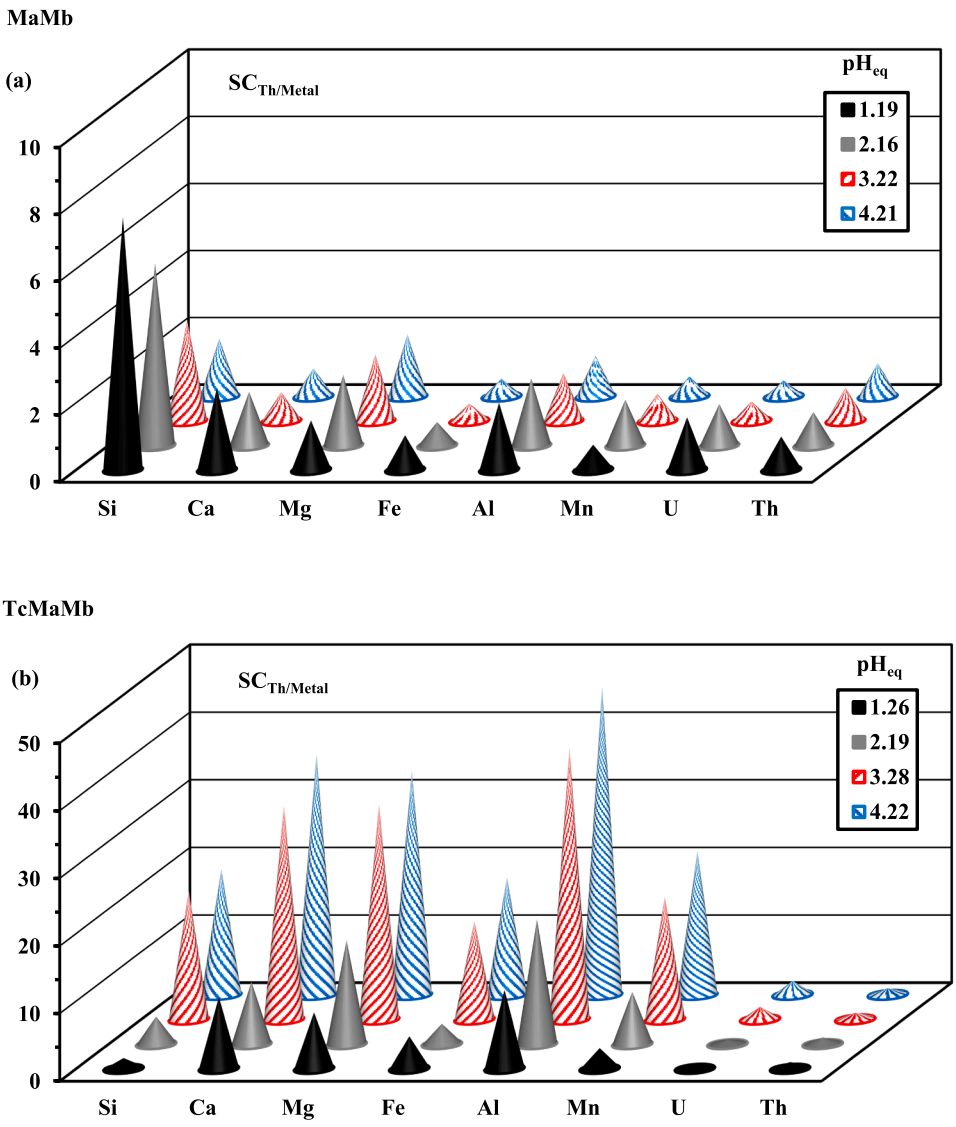

Fig. 8. Effect of pH on the selectivity coefficient ($SC_{Th/metal}$) for MaMb (a) and TcMaMb (b) sorbents for the treatment of pre-treated leachate (SD: 7.5 g L^{-1}; v: 210 rpm; time: 10 h; T: 21 ± 1 °C; $SC_{Th/Th} = 1$ as reference).

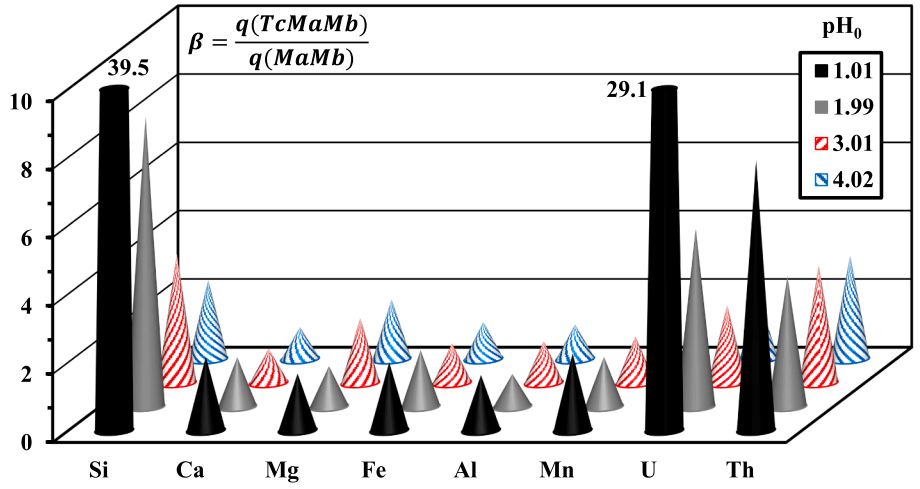

Fig. 9. Enhancement factor (β = q(TcMaMb)/q(MaMb)) for the treatment of pre-treated leachate (SD: 7.5 g L^{-1}; v: 210 rpm; time: 10 h; T: 21 ± 1 °C; for truncated cones (at β > 10) the true value is labelled, at pH_0 1.01).

values systematically remain below 0.13 L g^{-1}. In the case of pristine sorbent, despite the increase of the distribution ratio with the pH, the values remain systematically between 0.032 L g^{-1} (for Ca(II)) and 0.123 L g^{-1} (for Th(IV)), at pH_{eq} ≈4.2. The concentration effect of the sorbents is drastically increased by functionalization (together with the selective differentiation between Th(IV) and U(VI) and the other metal ions and metalloid). The cumulative sorption capacity increases with the pH (Fig. S20); though less marked at pH above 3. It is noteworthy that the difference between MaMb and TcMaMb tends to decrease with increasing pH. The deprotonation of reactive groups increases the sorption of competitor ions for MaMb, which, in turn, leads to the saturation of the sorbent and total sorption capacity is comparable with TcMaMb. This is consistent with the lack of selectivity of pristine MaMb sorbent. The beneficial effect of functionalization is highlighted in Fig. 9. The increase in the sorption capacity with functionalization (β coefficient) is marked at low pH value (reaching up to 29 for U(VI) and 8 for Th(IV)), though the levels for sorption capacities are strongly depreciated (compared with pH 4–5 data): strictly below 0.0165 mmol g^{-1} for MaMb and up to 0.0274 mmol g^{-1} for TcMaMb. The enhancement (i.e., β) at pH_0 4.02 (for higher sorption capacities) follows the trend:

Th(IV) [3.04] > Si(IV) [2.32] > U(VI) [1.86] ≈ Mg(II) [1.75] > Fe (III),Mn(II),Al(III),Ca(II) [1.09–0.93].

4. Conclusion

A new sorbent was prepared by the direct reaction of maleic anhydride with *N*,*N*'-methylenebisacrylamide (MaMb). This material, bearing carboxylic acid, tertiary amine and carboxyl groups, shows at pH_0 4 a maximum sorption capacity close to 0.6 mmol Th g^{-1}. The equilibrium (under selected experimental conditions) is reached in 120–180 min. The functionalization of MaMb by grafting thiocarbazide (to form TcMaMb) allows significantly improving the sorption performance: reduced equilibrium time (to 30 min), increasing of both the maximum sorption capacity (up to 1.36 mmol Th g^{-1}) and the Langmuir affinity coefficient (from 0.81 to 4.65 L $mmol^{-1}$). The grafting increases the density of reactive groups (amine and carbonyl) and brings additional amide and thiocarbonyl groups. However, some other important criteria are being improved as well. The chemical modification allows maintaining good sorption properties for at least five cycles: the loss at the fifth cycle does not exceed 1.8 % compared with initial step (against 7.8 % for pristine sorbent), while the desorption efficiency maintains systematically higher than 99.5 %. The stability of the sorbent is increased by chemical modification. However, one of the most interesting benefit of the functionalization concerns the selectivity of the sorbent for thorium (and uranium) against metalloids such as Si(IV), alkali-earth elements or base metals. While MaMb is characterized by the binding of a wide range of elements (from multi-component equimolar solutions), with comparable levels of sorption, the grafting of thiocarbazide strongly increases the preference of TcMaMb for thorium (and uranium(VI) that cannot be separated from Th(IV)). The functionalization poorly affects the sorption of competitor ions but contributes to 2–2.5-fold increase in total sorption capacity at pH_0 4–5. This study clearly demonstrates the superiority of the multifunctional sorbent for the removal of uranium and thorium, even from complex effluent such as pre-treated acidic ore leachate (after U sorption onto quaternary ammonium resin, and precipitation of iron and aluminum at mild acidic pH).

Based on these promising results, next step in the development of these materials would require designing the sorbent as spherical particles for enhanced applications in fixed-bed columns. Testing a larger number of re-uses would also contribute to the more accurate evaluation of the potential of these materials. For the application of TcMaMb in the treatment of nuclear effluents, it would be also necessary testing its stability under irradiation.

Declaration of Competing Interest

The authors declare that they have no known competing financial interests or personal relationships that could have appeared to influence the work reported in this paper.

Data availability

Data will be made available on request.

Acknowledgements

Y.W acknowledges the financial support of National Natural Science Foundation of China for supporting projects [U1967218, and 11975082] and the National Key R&D Program of China for the project [2022YFB3506100].

Appendix A. Supplementary data

Supplementary data to this article can be found online at https://doi.org/10.1016/j.cej.2023.142638.

References

[1] S. Perros, Le thorium : l'espoir d'une énergie nucléaire verte, in, Optima Energie, 2022.
[2] G.T. Lapidus, F.M. Doyle, Selective thorium and uranium extraction from monazite: II Approaches to enhance the removal of radioactive contaminants, Hydrometallurgy 155 (2015) 161–167.
[3] A.H. El-Afandy, A.M. Yousif, A.E. Mubark, Subsequent separation of niobium (Nb), thorium (Th), rare earth elements (REEs), zirconium (Zr), and uranium (U) from Abu Rusheid cataclastic concentrate, South Eastern Desert, Egypt, Radiochemistry 64 (2022) 257–267.
[4] N.T. Hung, L.B. Thuan, T.C. Thanh, N.T. Thuy, D.T.T. Tra, K. Do Van, M. Watanabe, P.Q. Minh, H.S. Than, N.D. Vuong, et al., Selective recovery of thorium and uranium from leach solutions of rare earth concentrates in continuous solvent extraction mode with primary amine N1923, Hydrometallurgy 213 (2022), 105933.
[5] J.H. Jeon, A.B.C. Sola, G.B. Park, J.-Y. Lee, H.-I. Kim, R.K. Jyothi, Development of a recovery process of thorium and possible separation of rare earths from Korean monazite, Geosyst. Eng. (2022), https://doi.org/10.1080/12269328.2022.2158496.
[6] N. Reynier, M. Courchesne, J. Basque, C. Laviolette, A. Demers, D. Lariviere, Thorium ion exchange separation from rare earth elements ore samples following a combined attrition and dissolution procedure, Miner. Eng. 175 (2022), 107284.
[7] S. Kursunoglu, S. Hussaini, S. Top, Z.T. Ichlas, H.S. Gokcen, S. Ozsarac, M. Kaya, Production of mixed rare earth oxide powder from a thorium containing complex Bastnasite ore, Powder Technol. 379 (2021) 641–654.
[8] F.A. Aydin, M. Soylak, A novel multi-element coprecipitation technique for separation and enrichment of metal ions in environmental samples, Talanta 73 (2007) 134–141.
[9] K.L. Ang, D. Li, A.N. Nikoloski, The effectiveness of ion exchange resins in separating uranium and thorium from rare earth elements in acidic aqueous sulfate media. Part 1. Anionic and cationic resins, Hydrometallurgy 174 (2017) 147–155.
[10] K.L. Ang, D. Li, A.N. Nikoloski, The effectiveness of ion exchange resins in separating uranium and thorium from rare earth elements in acidic aqueous sulfate media. Part 2. Chelating resins, Miner. Eng. 123 (2018) 8–15.
[11] J.T.M. Amphlett, S. Choi, S.A. Parry, E.M. Moon, C.A. Sharrad, M.D. Ogden, Insights on uranium uptake mechanisms by ion exchange resins with chelating functionalities: chelation vs. anion exchange, Chem. Eng. J. 392 (2020), 123712.
[12] B.M. Atia, Y.M. Khawassek, G.M. Hussein, M.A. Gado, M.A. El-Sheify, M.F. Cheira, One-pot synthesis of pyridine dicarboxamide derivative and its application for uranium separation from acidic medium, J. Environ. Chem. Eng. 9 (2021), 105726.
[13] M.F. Hamza, Y. Wei, M.S. Khalafalla, N.S. Abed, A. Fouda, K.Z. Elwakeel, E. Guibal, N.A. Hamad, U(VI) and Th(IV) recovery using silica beads functionalized with urea- or thiourea-based polymers – Application to ore leachate, Sci. Total Environ. 821 (2022), 153184.
[14] M. Karve, K. Pandey, Cyanex272 impregnated on Amberlite XAD-2 for separation and preconcentration of U(VI) from uranmicrolite (leachates) ore tailings, J. Radioanal. Nucl. Chem. 285 (2010) 627–633.
[15] B. Mahanty, P.K. Mohapatra, Highly efficient separation of thorium from uranium in nitric acid feeds by solid phase extraction using Aliquat 336, Sep. Purif. Technol. 237 (2020), 116318.
[16] R.B. Gujar, P.K. Mohapatra, M. Iqbal, J. Huskens, W. Verboom, Selective uptake of thorium(IV) from nitric acid medium using two extraction chromatographic resins based on diglycolamide-calix[4]arenes: application to thorium-uranyl separation in an actual sample, J. Chromatogr. A 1653 (2021), 462401.

[17] V. Beaugeard, J. Muller, A. Graillot, X. Ding, J.-J. Robin, S. Monge, Acidic polymeric sorbents for the removal of metallic pollution in water: a review, React. Funct. Polym. 152 (2020), 104599.
[18] L.-Y. Yuan, Z.-Q. Bai, R. Zhao, Y.-L. Liu, Z.-J. Li, S.-Q. Chu, L.-R. Zheng, J. Zhang, Y.-L. Zhao, Z.-F. Chai, et al., Introduction of bifunctional groups into mesoporous silica for enhancing uptake of thorium(IV) from aqueous solution, ACS Appl. Mater. Interfaces 6 (2014) 4786–4796.
[19] M.F. Cheira, Performance of poly sulfonamide/nano-silica composite for adsorption of thorium ions from sulfate solution, SN Appl. Sci. 2 (2020) 398.
[20] F. Zhang, K.-Q. Ma, Y. Li, Q. Ran, C.-Y. Yao, C.-T. Yang, H.-Z. Yu, S. Hu, S.-M. Peng, Selective separation of thorium from rare earths and uranium in acidic solutions by phosphorodiamidate-functionalized silica, Chem. Eng. J. 392 (2020), 123717.
[21] S. Alharthi, Sequestering of radioactive thorium from wastewater using highly porous silica monoliths, JOM 74 (2022) 1035–1043.
[22] M. Tuzen, A. Sari, T.A. Saleh, Synthesis, characterization and evaluation of carbon nanofiber modified-polymer for ultra-removal of thorium ions from aquatic media, Chem. Eng. Res. Des. 163 (2020) 76–84.
[23] C.E. Yilmaz, M.A.A. Aslani, C.K. Aslani, Removal of thorium by modified multi-walled carbon nanotubes: optimization, thermodynamic, kinetic, and molecular dynamic viewpoint, Prog. Nucl. Energy 127 (2020), 103445.
[24] Y. Wang, X. Hu, Y. Liu, Y. Li, T. Lan, C. Wang, Y. Liu, D. Yuan, X. Cao, H. He, et al., Assembly of three-dimensional ultralight poly(amidoxime)/graphene oxide nanoribbons aerogel for efficient removal of uranium(VI) from water samples, Sci. Total Environ. 765 (2021), 142686.
[25] K. Dev, R. Pathak, G.N. Rao, Sorption behaviour of lanthanum(III), neodymium (III), terbium(III), thorium(IV) and uranium(VI) on Amberlite XAD-4 resin functionalized with bicine ligands, Talanta 48 (1999) 579–584.
[26] A. Rahmani-Sani, A. Hosseini-Bandegharaei, S.H. Hosseini, K. Kharghani, H. Zarei, A. Rastegar, Kinetic, equilibrium and thermodynamic studies on sorption of uranium and thorium from aqueous solutions by a selective impregnated resin containing carminic acid, J. Hazard. Mater. 286 (2015) 152–163.
[27] D.X. He, N. Tan, X.M. Luo, X.C. Yang, K. Ji, J.W. Han, C. Chen, Y.Q. Liu, Preparation, uranium (VI) absorption and reuseability of marine fungus mycelium modified by the bis-amidoxime-based groups, Radiochim. Acta 108 (2020) 37–49.
[28] M.F. Hamza, E. Guibal, K. Althumayri, T. Vincent, X. Yin, Y. Wei, W. Li, New process for the sulfonation of algal/PEI biosorbent for enhancing Sr(II) removal from aqueous solutions - Application to seawater, Molecules 27 (2022) 7128.
[29] A.M. Atta, Z.F. Akl, Removal of thorium from water using modified magnetite nanoparticles capped with rosin amidoxime, Mater. Chem. Phys. 163 (2015) 253–261.
[30] S.D. Alexandratos, X.P. Zhu, M. Florent, R. Sellin, Polymer-supported bifunctional amidoximes for the sorption of uranium from seawater, Ind. Eng. Chem. Res. 55 (2016) 4208–4216.
[31] M.F. Hamza, J.-C. Roux, E. Guibal, Uranium and europium sorption on amidoxime-functionalized magnetic chitosan micro-particles, Chem. Eng. J. 344 (2018) 124–137.
[32] M. Ahmad, J. Wang, Z. Yang, Q. Zhang, B. Zhang, Ultrasonic-assisted preparation of amidoxime functionalized silica framework via oil-water emulsion method for selective uranium adsorption, Chem. Eng. J. 389 (2020), 124441.
[33] S.D. Alexandratos, X. Zhu, Polymer-supported aminomethylphosphinate as a ligand with a high affinity for U(VI) from phosphoric acid solutions: Combining variables to optimize ligand-ion communication, Solvent Extr. Ion Exch. 34 (2016) 290–295.
[34] C.E. Duval, W.A. Hardy, S. Pellizzeri, T.A. DeVol, S.M. Husson, Phosphonic acid and alkyl phosphate-derivatized resins for the simultaneous concentration and detection of uranium in environmental waters, React. Funct. Polym. 137 (2019) 133–139.
[35] D.A. Giannakoudakis, I. Anastopoulos, M. Barczak, E. Antoniou, K. Terpilowski, E. Mohammadi, M. Shams, E. Coy, A. Bakandritsos, I.A. Katsoyiannis, et al., Enhanced uranium removal from acidic wastewater by phosphonate-functionalized ordered mesoporous silica: Surface chemistry matters the most, J. Hazard. Mater. 413 (2021), 125279.
[36] P. Yang, Q. Liu, J. Liu, R. Chen, R. Li, X. Bai, J. Wang, Highly efficient immobilization of uranium(VI) from aqueous solution by phosphonate-functionalized dendritic fibrous nanosilica (DFNS), J. Hazard. Mater. 363 (2019) 248–257.
[37] M.O.A. El-Magied, A.S. Dhmees, A.A.M. Abd El-Hamid, E.M. Eldesouky, Uranium extraction by sulfonated mesoporous silica derived from blast furnace slag, J. Nucl. Mater. 509 (2018) 295–304.
[38] S. Song, K. Wang, Y. Zhang, Y. Wang, C. Zhang, X. Wang, R. Zhang, J. Chen, T. Wen, X. Wang, Self-assembly of graphene oxide/PEDOT:PSS nanocomposite as a novel adsorbent for uranium immobilization from wastewater, Environ. Pollut. 250 (2019) 196–205.
[39] M.F. Hamza, A.E. Mubark, Y. Wei, T. Vincent, E. Guibal, Quaternization of composite algal/PEI beads for enhanced uranium sorption-application to ore acidic leachate, Gels 6 (2020) 6020012.
[40] X.M. Li, F.F. Dong, Y.W. Huang, X.P. Zhi, Y.L. Shen, Synthesis of quaternary ammonium salt functionalized large-particle silica gel for removal of uranium, J. Radioanal. Nucl. Chem. 329 (2021) 171–177.
[41] S.D. Alexandratos, S.D. Smith, Intraligand cooperation in metal-ion binding by immobilized ligands: The effect of bifunctionality, J. Appl. Polym. Sci. 91 (2004) 463–468.
[42] X. Zhu, S.D. Alexandratos, Development of a new ion-exchange/coordinating phosphate ligand for the sorption of U(VI) and trivalent ions from phosphoric acid solutions, Chem. Eng. Sci. 127 (2015) 126–132.
[43] X. Nie, Y. Jiang, F. Dong, W. Cheng, J. Wang, C. Ding, M. Liu, Y. Zhang, X. Xia, Amide and phosphate groups modified bifunctional luffa fiber for highly efficient removal of U(VI) from real uranium wastewater, J. Radioanal. Nucl. Chem. 328 (2021) 591–604.
[44] G. Zhang, H. Fan, R.-Y. Zhou, W. Yin, R. Wang, M. Yang, Z. Xue, Y. Yang, J.-X. Yu, Decorating UiO-66-NH_2 crystals on recyclable fiber bearing polyamine and amidoxime bifunctional groups via cross-linking method with good stability for highly efficient capture of U(VI) from aqueous solution, J. Hazard. Mater. 424 (2022), 127273.
[45] Y. Li, X.-X. Li, Z.-Y. Wang, F. Zhang, Q. Wu, L.-T. Sha, Y. Wang, Z.-Y. Yan, Design and synthesis of a novel bifunctional polymer with malonamide and carboxyl group for highly selective separation of uranium (VI), Sep. Purif. Technol. 302 (2022), 122115.
[46] Z. Ahmad, Y. Li, S. Ali, J. Yang, F. Jan, Y. Fan, X. Gou, Q. Sun, J. Chen, Benignly-fabricated supramolecular poly(amidoxime)-alginate-poly(acrylic acid) beads synergistically enhance uranyl capture from seawater, Chem. Eng. J. 441 (2022), 136076.
[47] M.L. Dietz, E.P. Horwitz, L.R. Sajdak, R. Chiarizia, An improved extraction chromatographic resin for the separation of uranium from acidic nitrate media, Talanta 54 (2001) 1173–1184.
[48] J. Zhou, D. Wu, D. Guo, Optimization of the production of thiocarbohydrazide using the Taguchi method, J. Chem. Technol. Biotechnol. 85 (2010) 1402–1406.
[49] M. Szkudlarek, E. Heine, H. Keul, U. Beginn, M. Möller, Synthesis, characterization, and antimicrobial properties of peptides mimicking copolymers of maleic anhydride and 4-methyl-1-pentene, Int. J. Mol. Sci. 19 (2018) 2617.
[50] M.V. Lopez-Ramon, F. Stoeckli, C. Moreno-Castilla, F. Carrasco-Marin, On the characterization of acidic and basic surface sites on carbons by various techniques, Carbon 37 (1999) 1215–1221.
[51] W. Davies, W. Gray, A rapid and specific titrimetric method for the precise determination of uranium using iron(II) sulphate as reductant, Talanta 11 (1964) 1203–1211.
[52] K.J. Mathew, S. Bürger, S. Vogt, P. Mason, M.E. Morales-Arteaga, U.I. Narayanan, Uranium assay determination using Davies and Gray titration: an overview and implementation of GUM for uncertainty evaluation, J. Radioanal. Nucl. Chem. 282 (2009) 939–944.
[53] Z. Marczenko, M. Balcerzak, Chapter 39 - Rare-earth elements, in: Z. Marczenko, M. Balcerzak (Eds.), Analytical Spectroscopy Library, Elsevier, 2000, pp. 341–349.
[54] S.A.E.A. Mahmoud, W.M. Abdellah, H.A. Abu Khoziem, Mineralogy, geochemistry and leaching characteristics of the high-grade Th-U-Y zone of altered syenite at El Garra El Hamra, Southwestern Desert, Egypt, Miner. Metall. Process. 35 (2018) 230–240.
[55] N.T. Hung, L.T. Thuan, T.C. Thanh, M. Watanabe, D. Van Khoai, N.T. Thuy, H. Nhuan, P.Q. Minh, T.H. Mai, N.V. Tung, et al., Separation of thorium and uranium from xenotime leach solutions by solvent extraction using primary and tertiary amines, Hydrometallurgy 198 (2020), 105506.
[56] S.M. El Hady, A.R. Bakry, Selective recovery of lanthanides and uranium from xenotime mineral concentrate of Southwestern Sinai, Radiochemistry 64 (2022) 1–8.
[57] M.A. Metwally, M.E. Khalifa, M. Koketsu, Thiocarbohydrazides: Synthesis and reactions, Amer. J. Chem. 2 (2012) 38–51.
[58] A.A. Ibrahim, A.-E.-S. Abdel-Megied, M.S. Selim, H.H. Darweesh, M.M. Ayoub, New polymeric admixture for cement based on hyperbranched poly amide-ester with pentaerythritol core, ISRN Mater. Sci. 2013 (2013), 270987.
[59] M. Thommes, K. Kaneko, A.V. Neimark, J.P. Olivier, F. Rodriguez-Reinoso, J. Rouquerol, K.S.W. Sing, Physisorption of gases, with special reference to the evaluation of surface area and pore size distribution (IUPAC Technical Report), Pure Appl. Chem. 87 (2015) 1051–1069.
[60] K.S. Siddiqi, S. Khan, S.A.A. Nami, M.M. El-ajaily, Polynuclear transition metal complexes with thiocarbohydrazide and dithiocarbamates, Spectrochim. Acta, Part A 67 (2007) 995–1002.
[61] G.R. Burns, Metal complexes of thiocarbohydrazide, Inorg. Chem. 7 (1968) 277–283.
[62] D. Lin-Vien, N.B. Colthup, W.G. Fateley, J.G. Grasselli, APPENDIX 3 - A Summary of Characteristic Raman and Infrared Frequencies, in: D. Lin-Vien, N.B. Colthup, W. G. Fateley, J.G. Grasselli (Eds.), The Handbook of Infrared and Raman Characteristic Frequencies of Organic Molecules, Academic Press, San Diego, 1991, pp. 477–490.
[63] J. Coates, Interpretation of Infrared Spectra, A Practical Approach, in: R.A. Meyers (Ed.), Encyclopedia of Analytical Chemistry, John Wiley & Sons Ltd, Chichester, U. K., 2000, pp. 10815–10837.
[64] C.N.R. Rao, R. Venkataraghavan, The C=S stretching frequency and the "-N-C=S bands" in the infrared, Spectrochim. Acta 18 (1962) 541–547.
[65] N.B. Colthup, L.H. Daly, S.E. Wiberley, Introduction to Infrared and Raman Spectroscopy, 3rd. ed., Academic Press Inc, San Diego, CA (USA), 1990, p. 560.
[66] L. Zhou, Y. Wang, H. Zou, X. Liang, K. Zeng, Z. Liu, A.A. Adesina, Biosorption characteristics of uranium(VI) and thorium(IV) ions from aqueous solution using CaCl2-modified Giant Kelp biomass, J. Radioanal. Nucl. Chem. 307 (2016) 635–644.
[67] H.N. Sheikh, B.L. Kalsotra, K. Shree, Complexes of thorium(IV) salts with morpholinomethylurea and related ligands, J. Indian Chem. Soc. 80 (2003) 909–911.
[68] Y.A. Teterin, I.O. Utkin, I.V. Melnikov, A.M. Lebedev, A.Y. Teterin, K.E. Ivanov, A. S. Nikitin, L. Vukchevich, X-Ray photoelectron study of thorium silicate $ThSiO_4 \cdot nH_2O$ and uranium silicate $USiO_4 \cdot nH_2O$, J. Struct. Chem. 41 (2000) 965–971.
[69] S.A. Kobets, G.N. Pshinko, Factors affecting forms of finding Th(IV) in aqueous solutions, J. Water Chem. Technol. 36 (2014) 51–55.

[70] P.D. Bhalara, D. Punetha, K. Balasubramanian, Kinetic and isotherm analysis for selective thorium(IV) retrieval from aqueous environment using eco-friendly cellulose composite, Int. J. Environ. Sci. Technol. 12 (2015) 3095–3106.
[71] OCDE, N.E. Agency, Chemical Thermodynamics of Thorium, Volume 11, Issy-les-Moulineaux (France), 2008, 945 pp.
[72] B.A. Salah, M.S. Gaber, A.H.T. Kandil, The removal of uranium and thorium from their aqueous solutions by 8-hydroxyquinoline immobilized bentonite, Minerals 9 (2019) 626.
[73] M. Albayari, M.K. Nazal, F.I. Khalili, N. Nordin, R. Adnan, Biochar derived from *Salvadora persica* branches biomass as low-cost adsorbent for removal of uranium (VI) and thorium(IV) from water, J. Radioanal. Nucl. Chem. 328 (2021) 669–678.
[74] D. Humelnicu, C. Blegescu, D. Ganju, Removal of uranium(VI) and thorium(IV) ions from aqueous solutions by functionalized silica: kinetic and thermodynamic studies, J. Radioanal. Nucl. Chem. 299 (2014) 1183–1190.
[75] A.H. Orabi, A.-E.-S. Abdelhamid, H.M. Salem, D.A. Ismaiel, New adsorptive composite membrane from recycled acrylic fibers and *Sargassum dentifolium* marine algae for uranium and thorium removal from liquid waste solution, J. Radioanal. Nucl. Chem. 326 (2020) 1233–1247.
[76] J.-P. Simonin, On the comparison of pseudo-first order and pseudo-second order rate laws in the modeling of adsorption kinetics, Chem. Eng. J. 300 (2016) 254–263.
[77] M.A. Hubbe, S. Azizian, S. Douven, Implications of apparent pseudo-second-order adsorption kinetics onto cellulosic materials: a review, BioResources 14 (2019) 7582–7626.
[78] M.O. Abd El-Magied, A.I.L. Abd el Fatah, H. Mashaal, A. Tawfique, I.G. Alhindawy, E.S.A. Manaa, E.A. Elshehy, Fabrication of worm-like mesoporous silica monoliths as an efficient sorbent for thorium ions from nitrate media, Radiochemistry 64 (2022) 62–73.
[79] E. Mauerhofer, K.P. Zhernosekov, F. Rösch, Limiting transport properties of lanthanide and actinide ions in pure water, Radiochim. Acta 91 (2003) 473–478.
[80] M.W. Abdel Raouf, A.M. El-Kamash, Kinetics and thermodynamics of the sorption of uranium and thorium ions from nitric acid solutions onto a TBP-impregnated sorbent, J. Radioanal. Nucl. Chem. 267 (2006) 389–395.
[81] E. Metwally, Kinetic studies for sorption of some metal ions from aqueous acid solutions onto TDA impregnated resin, J. Radioanal. Nucl. Chem. 270 (2006) 559–566.
[82] S.I. Mohamady, Functionalization of magnetic-chitosan nanocomposite for enhancing Th(IV) ions sorption, Egypt. J. Chem. 64 (2021) 2095–2111.
[83] A.A. Al-Massaedh, F.I. Khalili, Removal of thorium(IV) ions from aqueous solution by polyacrylamide-based monoliths: equilibrium, kinetic and thermodynamic studies, J. Radioanal. Nucl. Chem. 327 (2021) 1201–1217.
[84] Y. Huang, H. Zheng, H. Li, Z. Zhang, C. Zhao, Q. Gou, Y. Liu, Highly effective and selective adsorption of thorium(IV) from aqueous solution using mesoporous graphite carbon nitride prepared by sol-gel template method, Chem. Eng. J. 410 (2021), 128321.
[85] A.E. Mubark, N.I. Falila, H.M. Salem, Use of modified cellulose sorbents for the extraction of Th(IV) ions from chloride solutions, Radiochemistry 63 (2021) 484–497.
[86] E. Kamal, G. Hamdy, I.A. El-Sabbagh, Highly efficient capture of Th(IV) from aqueous solutions using GO/TiO_2 nanocomposite, Egypt. J. Chem. 64 (2021) 1353–1362.
[87] C.F. Baes Jr., R.E. Mesmer, Hydrolysis of Cations, Wiley, NY, 1976, p. 489.
[88] S.Y. Bratskaya, A.Y. Ustinov, Y.A. Azarova, A.V. Pestov, Thiocarbamoyl chitosan: Synthesis, characterization and sorption of Au(III), Pt(IV), and Pd(II), Carbohydr. Polym. 85 (2011) 854–861.
[89] C. Ravindran, A.P.P. Kunnathulli, J.K. Maniath, A.M. Isloor, Fabrication of eggshell derived hydroxyapatite polymer composite membrane for efficient removal of thorium ions from aqueous solutions, Mater. Today: Proc. 43 (2021) 2140–2149.
[90] T.S. Anirudhan, S. Rijith, A.R. Tharun, Adsorptive removal of thorium(IV) from aqueous solutions using poly(methacrylic acid)-grafted chitosan/bentonite composite matrix: process design and equilibrium studies, Colloids Surf. A 368 (2010) 13–22.
[91] L.S. Ismail, F.I. Khalili, F.M. Abu Orabi, Thorium(IV) removal and recovery from aqueous solutions using modified silica nanoparticles with cysteine or methionine amino acids, Desalin. Water Treat. 196 (2020) 161–176.
[92] T.A. Saleh, A. Sari, M. Tuzen, Development and characterization of bentonite-gum arabic composite as novel highly-efficient adsorbent to remove thorium ions from aqueous media, Cellulose 28 (2021) 10321–10333.
[93] I. Persson, Hydrated metal ions in aqueous solution: How regular are their structures? Pure Appl. Chem. 82 (2010) 1901–1917.
[94] E. Nieboer, D.H.S. Richardson, The replacement of the nondescript therm "heavy-metals" by a biologically and chemically significant classification of metal ions, Environ. Pollut. Series B 1 (1980) 3–26.
[95] R.G. Pearson, Acids and bases 151 (1966) 172–177.
[96] C.S. Kedari, S.S. Pandit, P.M. Gandhi, Separation by competitive transport of uranium(VI) and thorium(IV) nitrates across supported renewable liquid membrane containing trioctylphosphine oxide as metal carrier, J. Membr. Sci. 430 (2013) 188–195.
[97] W.A. Kassab, Comparative study for leaching processes of uranium, copper and cadmium from gibbsite ore material of Talet Seleim, Southwestern, Sinai, Egypt, J. Radioanal. Nucl. Chem. 332 (2023) 273–287.